BIOCHEMISTRY

RAD54L2-mediated DNA damage avoidance pathway specifically preserves genome integrity in response to topoisomerase 2 poisons

Huimin Zhang[1]†, Yun Xiong[1]†, Yilun Sun[2]†, Jeong-Min Park[1], Dan Su[1], Xu Feng[1], Sarah Keast[1], Mengfan Tang[1], Min Huang[1], Chao Wang[1], Mrinal Srivastava[1], Chang Yang[1], Dandan Zhu[1], Zhen Chen[1], Siting Li[1], Ling Yin[1], Yves Pommier[2], Junjie Chen[1]*

Type II topoisomerases (TOP2) form transient TOP2 cleavage complexes (TOP2ccs) during their catalytic cycle to relieve topological stress. TOP2ccs are covalently linked TOP2-DNA intermediates that are reversible but can be trapped by TOP2 poisons. Trapped TOP2ccs block transactions on DNA and generate genotoxic stress, which are the mechanisms of action of TOP2 poisons. How cells avoid TOP2cc accumulation remains largely unknown. In this study, we uncovered RAD54 like 2 (RAD54L2) as a key factor that mediates a TOP2-specific DNA damage avoidance pathway. RAD54L2 deficiency conferred unique sensitivity to treatment with TOP2 poisons. RAD54L2 interacted with TOP2A/TOP2B and ZATT/ZNF451 and promoted the turnover of TOP2 from DNA with or without TOP2 poisons. Additionally, inhibition of proteasome activity enhanced the chromatin binding of RAD54L2, which in turn led to the removal of TOP2 from chromatin. In conclusion, we propose that RAD54L2-mediated TOP2 turnover is critically important for the avoidance of potential TOP2-linked DNA damage under physiological conditions and in response to TOP2 poisons.

INTRODUCTION

Type II topoisomerases (TOP2) function to relieve topological stresses during diverse cellular processes such as transcription, replication, and chromosome separation (*1*–*3*). TOP2 acts as a homodimer in a catalytic cycle that cleaves both DNA strands and religates these DNA ends later (*1*). The transiently formed double-stranded breaks (DSBs) open a gate for the passing of DNA segments. During the cleavage of DNA strands, TOP2 is covalently bound to the 5′ ends of DNA, forming the so-called TOP2 cleavage complexes (TOP2ccs) (*1*). TOP2ccs form transiently and are reversible. However, TOP2 poisons such as etoposide (ETO) and doxorubicin stabilize the covalently bound TOP2 on DNA, which blocks its displacement and inhibits the religation of broken DNA ends (*4*, *5*). ETO-trapped TOP2ccs are still reversible, as the removal of ETO leads to rapid resealing of DNA breaks and displacement of TOP2 from DNA (*6*, *7*).

Trapped TOP2-DNA cleavage complexes (TOP2ccs) block transactions on DNA and generate torsional and genotoxic stress (*8*, *9*). Several mechanisms have been suggested for TOP2cc removal (*10*). On one hand, trapped TOP2 protein is ubiquitinated and subjected to proteasome-mediated degradation (*11*), after which the residual peptides can be further hydrolyzed by tyrosyl-DNA phosphodiesterase 2 (TDP2) (*12*). Alternatively, it is reported that SUMOylation of trapped TOP2 by SUMO E3 ligase ZATT/ZNF451 modulates the conformation of TOP2ccs and facilitates the direct removal of TOP2ccs by TDP2 (*13*). In this case, ZATT/ZNF451 promotes both the accessibility and activity of TDP2 toward the TOP2-DNA covalent bonds (*13*). On the other hand, nucleolytic enzymes involved in DSB repair, like MRE11-RAD50-NBS1 (MRN) and C-terminal binding protein 1 (CtBP1) interacting protein (CtIP), can also cleave DNA strands in the vicinity of a trapped TOP2cc, releasing the entire TOP2 DNA-protein complex (*14*–*19*). Once trapped TOP2 proteins are removed, protein-free DNA breaks can then be recognized and repaired by major DSB repair pathways such as nonhomologous end joining (NHEJ) or homologous recombination (HR) (*20*).

Inappropriate processing and unfaithful resolution of trapped TOP2ccs are detrimental to cells. It has been shown that during TOP2cc resolution, proteasome mediated repair of TOP2cc is highly error prone, which can generate chromosome rearrangements and mutations, and promote genome instability and oncogenesis (*7*). Meanwhile, emerging evidence suggests that impaired TOP2 catalytic cycle is a main source of DNA damage under physiological conditions in the absence of TOP2 poison, which contributes to carcinogenesis (*21*–*23*). It is therefore important to understand the temporal regulation of TOP2 and TOP2cc removal.

Here, we performed whole-genome CRISPR-Cas9 screening with ETO treatment, which revealed that RAD54L2 is a key factor that mediates resistance to TOP2 poisons. RAD54L2 is also called ARIP4 (androgen receptor–interacting protein 4) (*24*, *25*). It is a member of SNF2-like family (*26*). RAD54L2 is one of these SNF2-related adenosine triphosphatases (ATPases) that are known to generate superhelical torsion within linear DNA fragments through its ATPase activity (*24*). We found that RAD54L2 deficiency conferred specific sensitivity to treatment with TOP2 poisons and showed additive sensitivity with TDP2 loss in response to ETO treatment. RAD54L2 interacts with TOP2A/TOP2B and ZATT/ZNF451 and promotes the turnover of TOP2 from DNA with or without TOP2 poison. Because RAD54L2-mediated TOP2 turnover reduces DNA damage and preserves genomic stability, we

[1]Department of Experimental Radiation Oncology, The University of Texas MD Anderson Cancer Center, Houston, TX 77030, USA. [2]Developmental Therapeutics Branch and Laboratory of Molecular Pharmacology, Center for Cancer Research, NCI, NIH, Bethesda, MD 20892, USA.
*Corresponding author. Email: jchen8@mdanderson.org
†These authors contributed equally to this work.

named this pathway a TOP2-specific DNA damage avoidance pathway, which functions not only under physiological conditions but also in response to treatment with TOP2 poisons. Moreover, our ETO screening, conducted in human embryonic kidney (HEK) 293A cells, showed comparable and consistent results with screenings conducted in retinal pigment epithelium-1 (RPE1) cells (*27*), which jointly provides a comprehensive view of DNA damage response to TOP2 poisons.

RESULTS

Suppression of Ring Finger Protein 4 and proteasome-mediated ubiquitination and degradation processes confers cellular resistance to TOP2 poisons

To determine potential regulators involved in the repair of trapped TOP2, we performed whole-genome CRISPR-Cas9 screens in both wild-type (WT) and TDP2-KO (knockout) human HEK293A cells, with or without TOP2 poison ETO (Fig. 1A). The screens were carried out with Toronto Knock Out Library v3 (TKOv3) as previously described (*28*, *29*). Data analyses were performed with a model-based analysis of genome-wide CRISPR/Cas9 knockout (MAGeCK) (table S1) (*30*). To identify potential candidates that confer hypersensitivity or resistance to ETO treatment, drug Z was used to compare the ETO-treated group and not-treated (NT) group (table S2) (*31*). Consistent with previous reports (*27*, *29*), ZATT/ZNF451 and ABCC1 ranked as the top hits that conferred ETO hypersensitivity in TDP2-KO cells (Fig. 1B). ABCC1, which is also called multidrug resistance protein-1 (MRP1), is a member of the ABC transporter family and a unidirectional efflux transporter for many xenobiotics including anticancer drugs such as ETO (*32*). ZATT/ZNF451 has been shown to catalyze the direct removal of TOP2ccs by TDP2 (*13*, *33*). In addition, ZATT/ZNF451 may also have TDP2-independent functions during TOP2 mediated DNA damage repair and in response to replication stress (*13*, *29*, *33*, *34*). On the other side, depletion of TOP2A, the main target of ETO in human cells, enhanced cellular resistance to drug treatment. These data indicate that our results are highly reliable.

To elucidate the functional pathways that responded to ETO treatment, we next analyzed the screening results performed in WT and TDP2-KO cells together (Fig. 1, C and D). We found that, as expected, DNA repair, DSB repair, and DSB repair via HR pathways are the top-ranked functional pathways that confer cellular sensitivity to ETO treatment (Fig. 1, C and D). A deficiency of genes involved in negative regulation of transcription enhanced cellular sensitivity while a loss of genes participated in positive regulation of transcription made cells more resistant to ETO. This suggests that there is a tight correlation between transcription and ETO treatment, which may be due to the involvement of TOP2 in transcription regulation.

In agreement with a previous study (*7*), we found that depletion of proteasome-mediated ubiquitin-dependent protein catabolic process conferred profound cellular resistance to ETO treatment (Fig. 1, C and D). It has been long recognized that proteasome mediated degradation of trapped TOP2ccs exposes TOP2 induced DSBs and is important for the removal of TOP2ccs by TDP2 or other repair pathways (*35*, *36*). Thus, inhibition of proteasomal activity should suppress the repair of TOP2ccs following ETO treatment, as previously reported (*11*, *37*). However, the previous findings (*7*) and our screening data indicate that the proteasome-mediated pathway appears to play a negative role in regulating cellular sensitivity to ETO treatment, because depletion of these genes/proteins led to resistance but not sensitivity to ETO treatment as anticipated.

Ring Finger Protein 4 (RNF4), one of the top-ranked hits on the resistance direction, is a Small Ubiquitin-like Modifier (SUMO)–targeted ubiquitin ligase (STUBL), which ubiquitylates SUMOylated Topoisomerase DNA protein complexes (TOP-DPCs) for their subsequent degradation by the proteasome (*7*, *11*). Consistent with the earlier study (*7*), we found that knocking down of RNF4 in both WT and TDP2-KO cells reduced DNA damage response following ETO treatment (fig. S1A). Pretreating cells with proteasome inhibitor MG132 further suppressed the ETO induced DNA damage response (fig. S1A). It was reported previously that RNF4 is epistatic with the proteasome with regarding to TOP2cc degradation (*7*). The further suppression of DNA damage response caused by combined depletion of RNF4 and proteasome inhibition here may be due to incomplete depletion of RNF4 by small interfering RNA (siRNA). An alternative explanation is that there may be other enzymes that mediate the ubiquitination of TOP2cc for proteasome degradation, which has also been suggested by the early report (*7*). Again, as expected from our screening results, RNF4 knockdown made both WT and TDP2-KO cells more resistant to ETO (Fig. 1, E and F, and fig. S1B), which is consistent with the findings reported in mouse embryonic fibroblasts (*7*). On the other hand, knocking down of RNF4 conferred cellular sensitivity to hydroxyurea (HU) and cisplatin treatment (Fig. 1E). We did not observe any sensitivity or resistance toward the TOP1 poison camptothecin (CPT) with or without RNF4 knockdown (Fig. 1E).

To determine whether this unique effect of RNF4 loss in promoting resistance to TOP2 poisons is due to the particular cell line we used here, we reanalyzed the results of a large-scale genetic study of DNA damage response performed in RPE1 cells (*27*). We found that RNF4 also ranked at the top on the resistance direction of ETO (*27*). Further analysis showed that depletion of *RNF4* gene showed a preferential resistance toward DNA damage caused by doxorubicin, pyridostatin, and ETO (fig. S1C), which all involve TOP2 trapping. This pattern of drug sensitivity of *RNF4* is similar to that of *TOP2A* gene (fig. S1D), indicating that RNF4 depletion specifically leads to cellular resistance to TOP2 poisons.

These results further confirmed the previous findings and agree with their hypothesis (*7*), i.e., suppression of the proteasome-mediated processing of TOP2ccs allows TOP2cc reversal and avoids the formation of irreversible TOP2cc intermediates, which result in DNA breaks, DNA damage response, and cytotoxicity (fig. S1E). RNF4 was reported to function as a STUBL for both TOP1- and TOP2-DPCs (*11*). However, our results and analysis of RPE1 data revealed that depletion of RNF4 selectively conferred cellular resistance to TOP2 poisons, but not to TOP1 poison (Fig. 1E and fig. S1, C and D), suggesting that RNF4 may have a distinctive role in the removal of TOPccs that requires further investigation.

Depletion of RAD54L2 endows unique cellular sensitivity to TOP2 poisons

The next question is what cells use to deal with trapped TOP2ccs to avoid proteasome-mediated processing of TOP2ccs and therefore promote cell viability especially in response to ETO treatment. Notably, we found that RAD54L2 ranked as a top candidate in

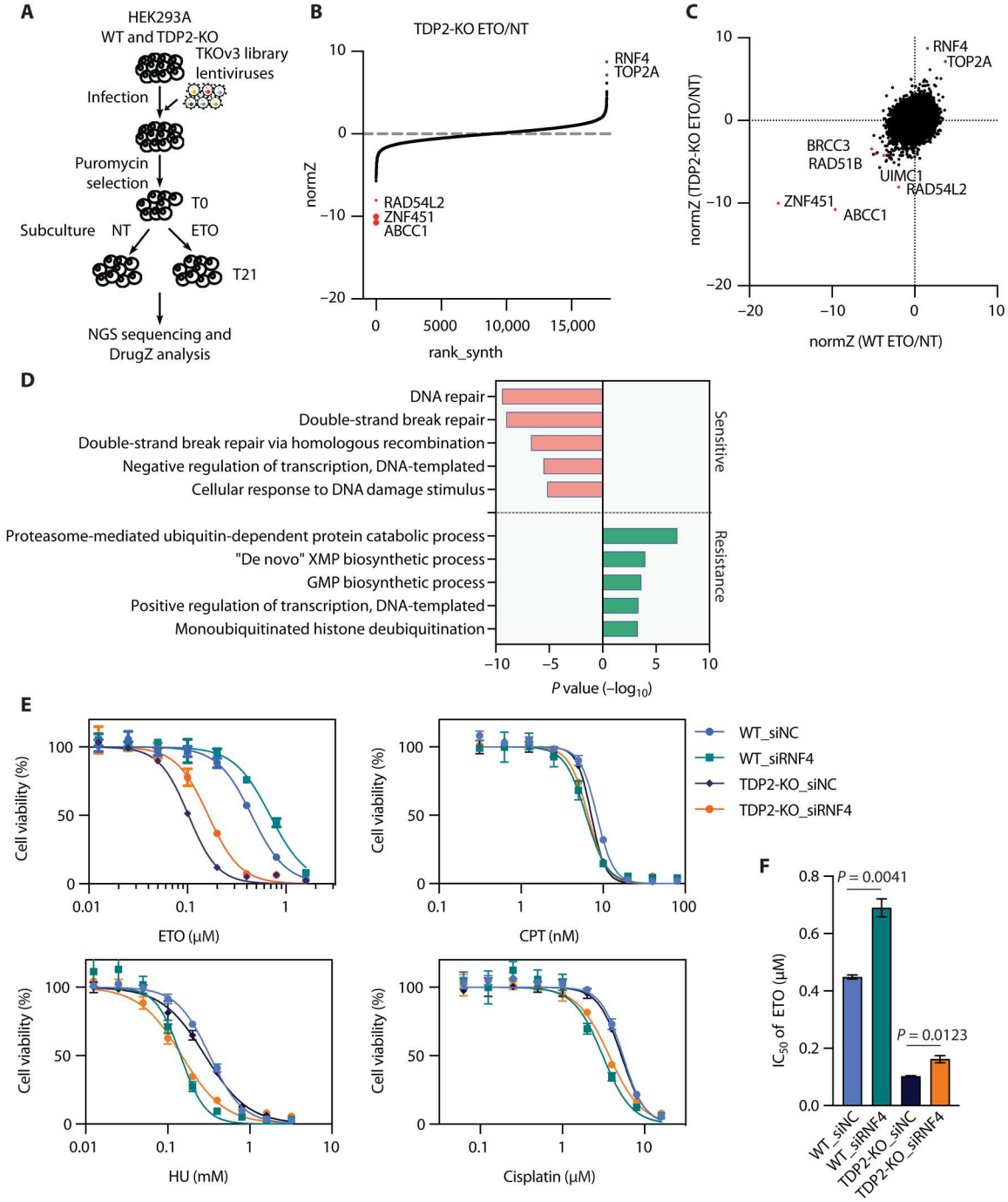

Fig. 1. Suppression of RNF4 and proteasome-mediated ubiquitination and degradation processes confers cellular resistance to TOP2 poison. (**A**) Schematic of the whole-genome CRISPR-Cas9 screens performed in HEK293A WT and TDP2-KO cells with Toronto Knock Out Library v3 (TKOv3). ETO (40 nM) was used for screening. NGS, next-generation sequencing. NT, not-treated. (**B**) Ranking of ETO coessential genes on the basis of drug Z analysis of the results of CRISPR/Cas9-based screening in HEK293A TDP2-KO cells. The *z*-score was used to define a possible synthetic lethal interaction with ETO. All genes targeted by the TKOv3 were scored according to the fold change of levels of their sgRNAs. The ETO-treated group and NT group in WT cells were compared. Genes whose loss of function led to ETO sensitivity appear on the left side, with a minus *z*-score, and genes whose loss of function led to ETO resistance appear on the right side, with a positive *z*-score. (**C**) Combinational comparison of ETO coessential genes between HEK293A WT and TDP2-KO cells. The *z*-scores from screening in HEK293A WT (*29*) and TDP2-KO cells were used. (**D**) Gene ontology clustering analysis of genes whose loss of function led to ETO sensitivity or resistance ($P < 0.01$) in WT and TDP2-KO cells was performed with DAVID Bioinformatics Resources 6.8, NIAID/NIH (https://david.ncifcrf.gov/summary.jsp). The top five enriched biological process were presented. (**E**) WT and TDP2-KO cells were transfected with siNC (non-targeting control) or siRNAs targeting RNF4. Cell proliferation was measured using a CellTiter-Glo assay after 4 days in the presence of the indicated concentrations of ETO, CPT, HU, or cisplatin. Data are presented as the mean ± SD ($n = 3$). (**F**) A two-tailed unpaired *t* test was used for statistical analysis of the IC50 of ETO treatment of each cell line in (E).

screens performed in TDP2-KO cells (Fig. 1B). RAD54L2 loss also conferred ETO sensitivity in WT cells (Fig. 1C), although not as strong as that in TDP2-KO cells.

RAD54L2 is a member of SNF2-like family and is an SNF2-related ATPase (*24*, *26*). To confirm the screening results, we generated RAD54L2-KO in both WT and TDP2-KO background using three different sgRNAs and confirmed the sensitivity of these KO cells toward ETO treatment (Fig. 2, A to C). In addition, in agreement with our screening results, RAD54L2 loss enhanced cellular sensitivity to ETO treatment in TDP2-KO cells (Fig. 2, A to C), indicating that RAD54L2 may operate in a pathway that differs from that of TDP2. RAD54L2 loss also conferred ETO hypersensitivity in HeLa WT and HeLa TDP2-KO cells (fig. S2, A and B). Next, we reanalyzed the drug response of RAD54L2 depletion published in RPE1 cells (*27*). We found that RAD54L2 deficiency showed strong sensitivity toward doxorubicin, ETO, and pyridostatin treatments (fig. S2C), similar to that of ZATT/ZNF451 and TDP2 (fig. S2C). In agreement with these screening results, loss of RAD54L2 conferred hypersensitivity to doxorubicin in both WT and TDP2-KO cells (Fig. 2D and fig. S2D). Two clones with RAD54L2 loss showed profound sensitivity to pyridostatin, while one clone only showed a slight difference (Fig. 2E and fig. S2E). Moreover, RAD54L2 loss showed additive effect with TDP2 loss in response to pyridostatin in all three clones (Fig. 2E and fig. S2E). Loss of RAD54L2 did not make these cells more sensitive to TOP2 activity inhibitor ICRF-187 (Fig. 2F). In addition, RAD54L2 loss did not lead to profound sensitivity to TOP1 poison CPT (fig. S3A), ionizing radiation (IR) (fig. S3B), or HU treatment (fig. S3C).

We then checked the DNA damage response following ETO treatment. As shown in Fig. 2G, depletion of RAD54L2 enhanced ETO induced phosphorylation of DNA-PKcs-S2056, ATM-S1981, KAP1-S824, RPA32-S4/8, and H2AX-S139 when comparing to those in WT cells. Phosphorylation of CHK2-T68 increased at early time points but decreased at late time points. Similar phenomena have been observed in our previous studies with TOP1 poison CPT (*28*), in which we reasoned that the hyperactivation of DNA-dependent protein kinase (DNA-PK) may somehow inhibit CHK2-T68 phosphorylation by ATM. TDP2/RAD54L2-DKO cells also triggered stronger phosphorylation of DNA-PKcs-S2056 and H2AX-S139 than those in TDP2-KO cells after ETO treatment (fig. S4A). The enhanced DNA damage response in cells with RAD54L2 and/or TDP2 loss was reduced or abolished by pretreating cells with proteasome inhibitor MG132, suggesting that proteasomal activity is also required for triggering the enhanced DNA damage response after ETO treatment in these cells.

Next, we used fluorescence-activated cell sorting (FACS) to analyze the phosphorylated H2AX-S139 signal. Consistent with Western blotting results, the phosphorylated H2AX-S139 signal increased with RAD54L2 loss after ETO treatment (Fig. 2, H and I, and fig. S4, B and C). We also observed a mild but reproducible increase of phosphorylated H2AX-S139 signal without ETO treatment (Fig. 2, H and I, and fig. S4, B and C), suggesting heightened endogenous DNA damage in cells with RAD54L2 loss. The unique ETO induced hypersensitivity and enhanced DNA damage response upon RAD54L2 loss suggest a specific function of RAD54L2 in the prevention and/or removal of TOP2ccs.

As RAD54L2 is related to HR proteins RAD54L and RAD54B (*38*), we also determined whether RAD54L2 is involved in HR repair using the DSB-induced HR repair reporter Direct repeat green fluorescent protein (DR-GFP). Knocking down of RAD54L2 did not notably affect HR repair efficiency (fig. S5, A and B), which suggests that RAD54L2 is not a key factor involved in HR. Depletion of RAD51 nearly abolished all HR-dependent repair (fig. S5, A and B). A slight additive effect was seen when further depleting RAD54L2 (fig. S5, A and B), which may be due to varied siRNA-mediated knockdown efficiency especially in cells treated with one or both siRNAs. Thus, we conclude that RAD54L2 likely plays no or minimal role in HR repair.

RAD54L2 interacts with TOP2A, TOP2B, and ZATT/ZNF451

To investigate mechanistically how RAD54L2 may be involved in the regulation of TOP2, we integrated the genetic and protein interaction data of TOP2A, TOP2B, ZATT/ZNF451, and RAD54L2 available from the Biological General Repository for Interaction Datasets (BioGRID) database. We found a strong connection between RAD54L2 and TOP2A, TOP2B, and ZATT/ZNF451 through proteins involved in SUMOylation (fig. S5C). To determine the potential interaction among these proteins, we overexpressed S protein-FLAG-Streptavidin binding peptide (RAD54L2-SFB) in the cell and conducted a coimmunoprecipitation assay. Endogenous ZATT/ZNF451, TOP2A, and TOP2B specifically immunoprecipitated with RAD54L2 (Fig. 3A). Reverse coimmunoprecipitations with overexpressed SFB-ZATT/ZNF451, SFB-TOP2A, and SFB-TOP2B also specifically coimmunoprecipitated RAD54L2 from cell extracts (Fig. 3, B to D). These results indicate that RAD54L2 interacts with TOP2A, TOP2B, and ZATT/ZNF451. Next, we confirmed these interactions in cells using a proximity ligation assay (PLA), which revealed that RAD54L2 was detected in the proximity of TOP2A and ZATT/ZNF451 in the cell (Fig. 3, E and F).

To examine whether RAD54L2 can directly interact with TOP2, we expressed recombinant RAD54L2 and TOP2A proteins in insect cells and purified these proteins (Fig. 3G). Benzonuclease and high-salt buffer were used separately to eliminate potential DNA and protein contamination during the protein preparation/purification process. RAD54L2 was specifically pulled down by 3FLAG-TOP2A (Fig. 3G), indicating a direct interaction between RAD54L2 and TOP2A in vitro.

RAD54L2 interacts with SUMOylated proteins

To further illustrate the interaction between RAD54L2 and TOP2A, TOP2B, and ZATT/ZNF451, we made a series of deletion mutants of RAD54L2 and examined their interactions with TOP2A, TOP2B, and ZATT/ZNF451. We found that deletion of amino acids 87 to 291, 292 to 513, 514 to 891, 728 to 892, and 892 to 1314 of RAD54L2 all reduced or abolished their interaction with TOP2A, TOP2B, and ZATT/ZNF451 (Fig. 4A), suggesting that the interactions of RAD54L2 with TOP2A, TOP2B, and/or ZATT/ZNF451 could be mediated by multidomains. On the other hand, we observed a substantial increase of the interaction between $RAD54L2^{1–86}$ or $RAD54L2^{1315–1467}$ with TOP2A and TOP2B (Fig. 4A), indicating additional regulation of the interaction between RAD54L2 and TOP2A/TOP2B. Moreover, we found that the interaction-compromised mutants could not rescue the ETO sensitivity caused by RAD54L2 loss (fig. S6, A and B), demonstrating the importance of protein interactions for RAD54L2 function.

The inability to find a specific interaction domain within RAD54L2 suggests that the interactions between RAD54L2 and TOP2A, TOP2B, and/or ZATT/ZNF451 could be multifaceted. In

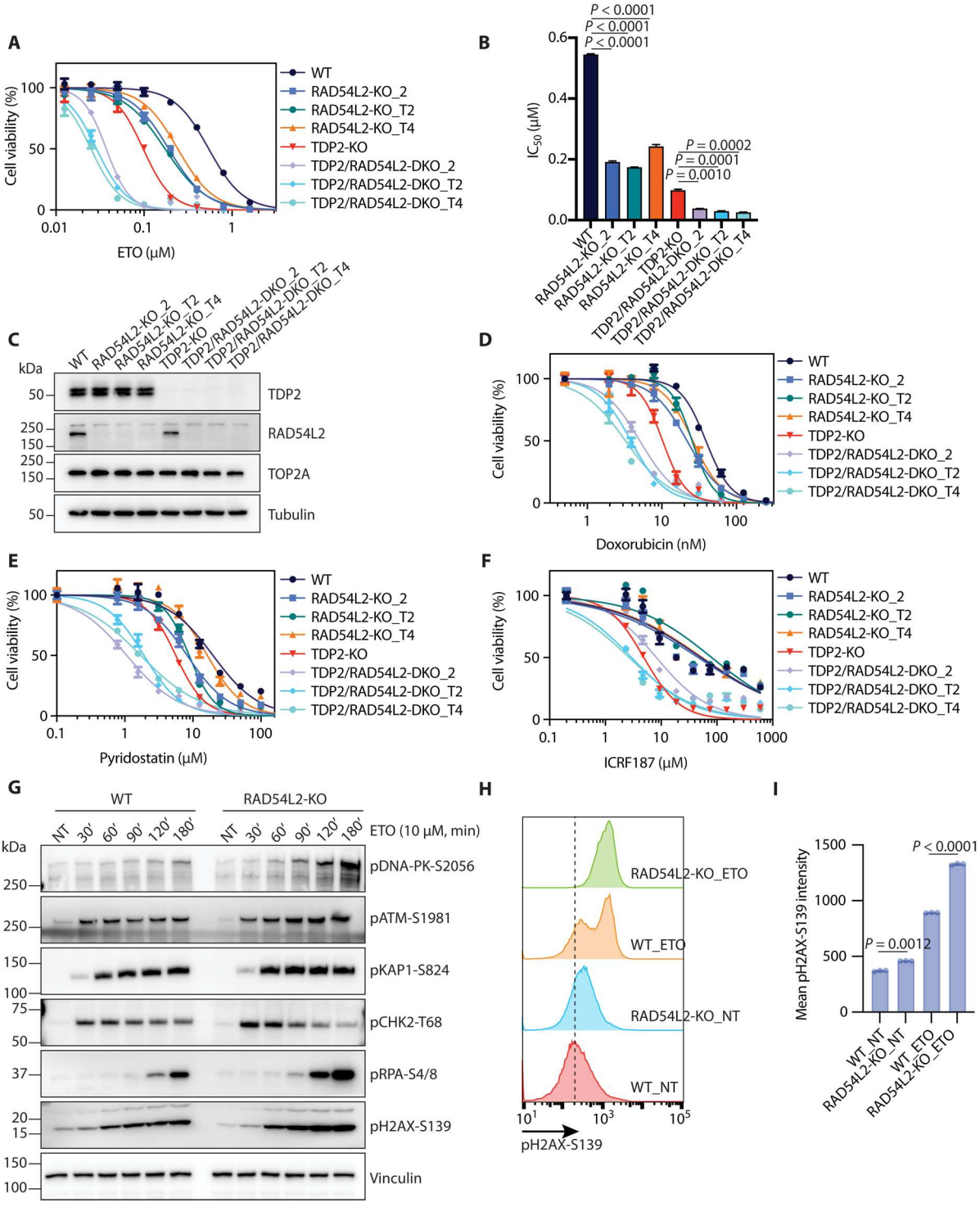

Fig. 2. Depletion of RAD54L2 endows unique cellular sensitivity to treatment with TOP2 poisons. (**A**) Proliferation of WT, TDP2-KO, RAD54L2-KO, and TDP2/RAD54L2-DKO cells were measured using a CellTiter-Glo assay after 4 days in the presence of indicated concentration of ETO. Data are presented as the mean ± SD (n = 3). (**B**) A two-tailed unpaired t test was used for statistical analysis of the IC50 of ETO treatment of each cell line in (A). (**C**) Western blotting showing TDP2 and RAD54L2 depletion in HEK293A cells. (**D** to **F**) Proliferation of WT, TDP2-KO, RAD54L2-KO, and TDP2/RAD54L2-DKO cells were measured using a CellTiter-Glo assay after 4 days in the presence of indicated concentration of doxorubicin (D), pyridostatin (E), and ICRF-187 (F). Data are presented as the mean ± SD (n = 3). (**G**) WT and RAD54L2-KO cells were treated with 10 μM ETO for the indicated times. Whole-cell extracts (WCEs) were prepared and subjected to Western blotting with the indicated antibodies. (**H**) A flow cytometry analysis of pH2AX-S139 intensity in WT and RAD54L2-KO cells that were either NT or treated with 4 μM ETO for 2 hours. (**I**) Quantification of (H). Mean pH2AX-S139 intensity from three independent experiments were shown in a bar chart (mean ± SD, n = 3). An unpaired t test with Welch's correction was used for statistical analysis.

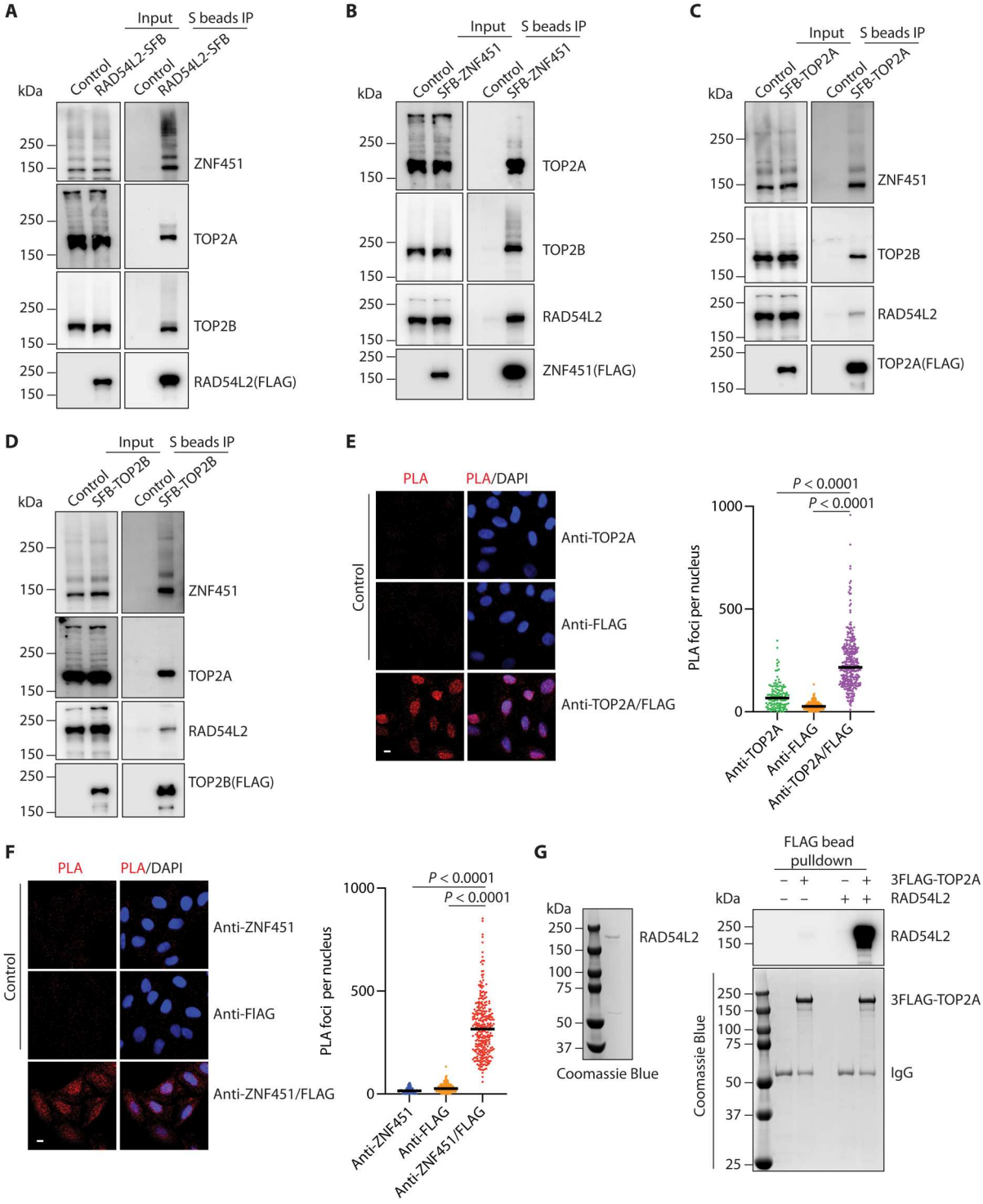

Fig. 3. RAD54L2 interacts with TOP2A/TOP2B and ZNF451. (**A** to **D**) HEK293A WT cells were either transfected with constructs encoding RAD54L2-SFB (A), SFB-ZNF451 (B), SFB-TOP2A (C), SFB-TOP2B (D), or empty vector as control and were subjected to immunoprecipitation (IP) with S beads. Western blotting was conducted with antibodies as indicated. (**E**) Representative confocal microscopy images from a TOP2A/RAD54L2-SFB (FLAG) PLA experiment. Scale bar, 10 μm. Quantification of indicated PLA foci in per nucleus was shown. The median number was indicated. (**F**) Representative confocal microscopy images from a ZNF451/RAD54L2-SFB (FLAG) PLA experiment. Scale bar, 10 μm. Quantification of indicated PLA foci in per nucleus was shown. The median number was indicated. (**G**) Coomassie Blue staining of purified RAD54L2 protein from insect cells was shown. Insect cell expressed 3FLAG-TOP2A was bound to FLAG-beads and subjected to washes with buffer that containing benzonuclease or high salt to eliminate contaminations from DNA or nonspecific proteins. Purified RAD54L2 (1 μg) was then mixed with FLAG-beads only or FLAG-beads bound with 3FLAG-TOP2A in NETN-100 lysis buffer for 2 hours. Beads were washed with NETN-100 lysis buffer three times and subjected to Western blotting with RAD54L2 antibody. Coomassie Blue staining was presented to show the bound 3FLAG-TOP2A on beads.

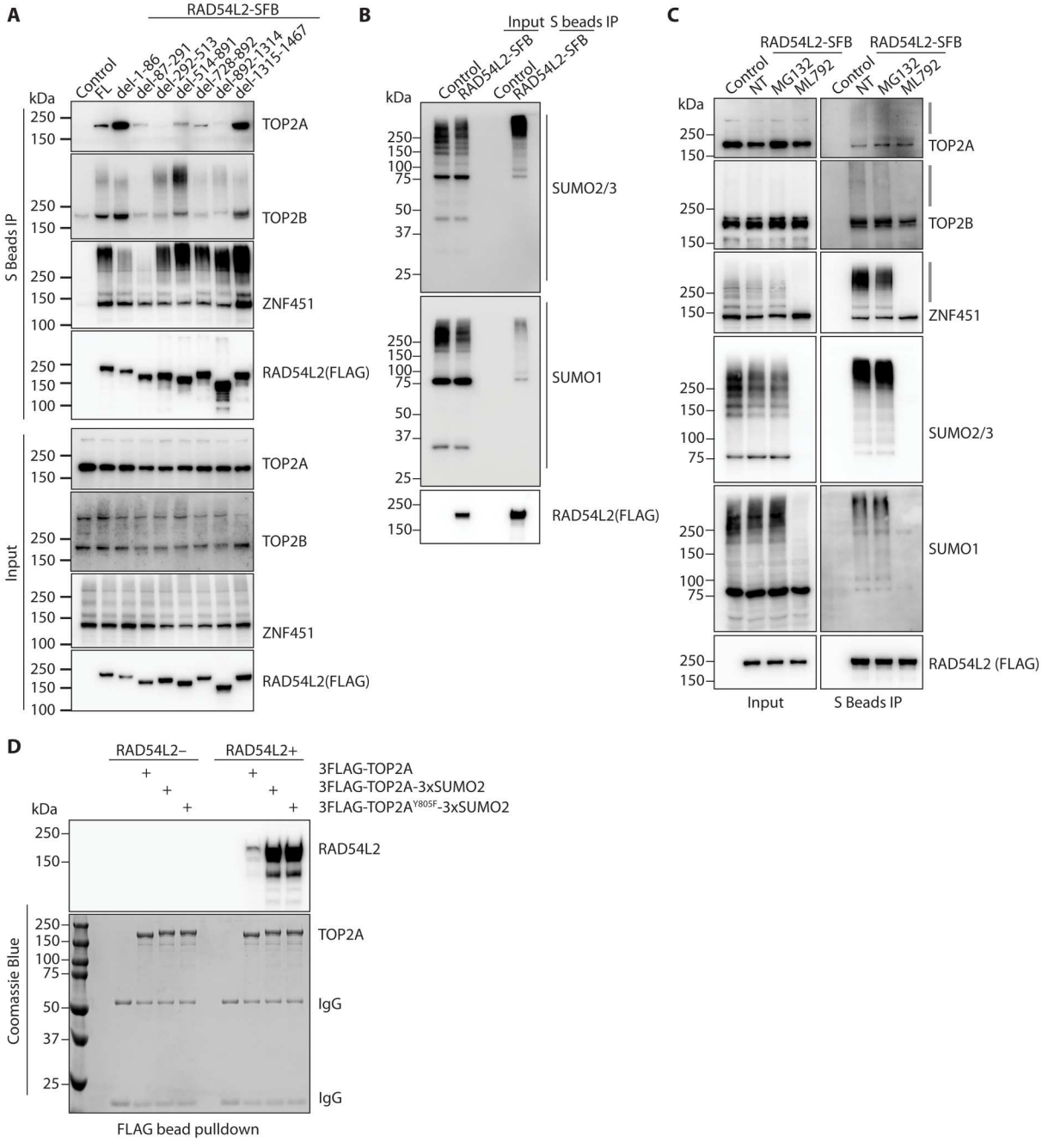

Fig. 4. RAD54L2 interacts with SUMOylated proteins. (**A**) HEK293A WT cells were transfected with constructs encoding RAD54L2-SFB or its deletion variants and were subjected to pull down with S beads. Western blotting was conducted with antibodies as indicated. (**B**) HEK293A WT cells were either transfected with constructs encoding RAD54L2-SFB or empty vector as control and were subjected to immunoprecipitation with S beads. Western blotting was conducted with antibodies as indicated. (**C**) HEK293A WT cells were either transfected with constructs encoding RAD54L2-SFB or empty vector as control. Cells were then treated with 10 μM MG132 or 10 μM ML-792 for 1 hour before subjected to immunoprecipitation with S beads. Western blotting was conducted with antibodies as indicated. The gray line indicates modified forms of TOP2A, TOP2B, or ZNF451. (**D**) Insect cell expressing 3FLAG-TOP2A, 3FLAG-TOP2A-3xSUMO2, and 3FLAG-TOP2A^{Y805F}-3xSUMO2 was bound to FLAG-beads and subjected to washes with buffer that containing benzonuclease or high salt to eliminate contaminations from DNA or nonspecific proteins. Purified RAD54L2 (1 μg) was then mixed with FLAG-beads only or FLAG-beads bound with 3FLAG-TOP2A, 3FLAG-TOP2A-3xSUMO2, or 3FLAG-TOP2A^{Y805F}-3xSUMO2 in NETN-100 lysis buffer for 2 hours. Beads were washed with NETN-100 lysis buffer three times and subjected to Western blotting with RAD54L2 antibody. Coomassie Blue staining was presented to show the bound 3FLAG-TOP2A, 3FLAG-TOP2A-3xSUMO2, or 3FLAG-TOP2A^{Y805F}-3xSUMO2 on beads.

coimmunoprecipitation assays, some slow migrated forms of TOP2A, TOP2B, and ZATT/ZNF451 were immunoprecipitated with RAD54L2 (Figs. 3A and 4A), which were potentially modified forms of these proteins. The deletion mutants of RAD54L2 showed different interactions with modified or unmodified proteins (Fig. 4A). Deletion of amino acids 87 to 291, 728 to 892, 892 to 1314, or 1315 to 1467 of RAD54L2 reduced its interaction with modified TOP2B, while depletion of amino acids 514 to 891 increased its interaction with modified TOP2B (Fig. 4A). The RAD54L2$^{del87–291}$ mutant also showed substantial reduced interaction with the modified forms of ZATT/ZNF451 (Fig. 4A). These observations indicate that the interactions between RAD54L2 and TOP2A, TOP2B, and/or ZATT/ZNF451 may also be mediated by protein modifications, perhaps SUMOylation, as suggested by BioGRID data (fig. S5C). RAD54L2 has been independently identified in multiple proteomic studies as SUMO-interacting proteins (*39*–*41*). Thus, we investigated the ability of RAD54L2 to interact with SUMOylated proteins and found that RAD54L2 could specifically coimmunoprecipitate SUMO1 and SUMO2/3 modified proteins (Fig. 4B). Pretreating cells with SUMO-activating enzyme inhibitor ML-792 abolished all SUMOylation events in the cell (Fig. 4C). Accordingly, no modified forms of TOP2A, TOP2B, and ZATT/ZNF451 were detected or coprecipitated with RAD54L2 after ML-792 treatment (Fig. 4C), suggesting that the modified forms coprecipitated with RAD54L2 could be SUMOylated TOP2A, TOP2B, and ZATT/ZNF451. RAD54L2$^{del87–291}$, which diminished its interaction with modified forms of TOP2B and ZATT/ZNF451 (Fig. 4A), also abolished its interaction with SUMOylated proteins (fig. S6C), further demonstrating that those modifications could be SUMOylation.

ML-792 treatment did not abolish the interaction between RAD54L2 and nonmodified forms of TOP2A, TOP2B, and ZATT/ZNF451(Fig. 4C), suggesting that RAD54L2 can interact with both SUMOylated and non-SUMOylated TOP2A, TOP2B, and ZATT/ZNF451. In addition, inhibition of proteasome activity did not affect the global interactions between RAD54L2 and TOP2A, TOP2B, or ZATT/ZNF451 (Fig. 4C). We next generated 3xSUMO2-fused TOP2A and tested its interaction with RAD54L2 in vitro. Notably, fusion with 3xSUMO2 enhanced the interaction between TOP2A and RAD54L2 (Fig. 4D), indicating a direct binding of RAD54L2 to SUMO2 and enhanced interaction between RAD54L2 and TOP2A-3xSUMO2 fusion protein in vitro. We suspect that these data also suggest that RAD52L2 preferentially binds to SUMOylated TOP2. When comparing the relative abundance of SUMOylated and non-SUMOylated forms of TOP2A, TOP2B, and ZATT/ZNF451 from input and S beads immunoprecipitation fractions, we found that the SUMOylated forms of these proteins were enriched more than the unmodified proteins (Figs. 3A and 4, A and C).

Together, these observations suggest multifaceted interactions between RAD54L2 and TOP2A, TOP2B, and ZATT/ZNF451, probably through both the direct binding of RAD54L2 to these proteins and the association of RAD54L2 with SUMOylated forms of these proteins. We noticed that a high proportion of endogenous ZATT/ZNF451 was SUMOylated, while only very limited amount of TOP2A/TOP2B were SUMOylated (Fig. 4, A and C). It has been reported that ZATT/ZNF451 exhibited autoSUMOylation activity and catalyzed polySUMOylation of TOP2A (*13*, *34*). In addition, TOP2ccs were found to be SUMOylated by ZATT/ZNF451 and PIAS4 before ubiquitylation by RNF4, which lead to their proteasome-mediated degradation (*11*, *13*). The preference binding of RAD54L2 to SUMOylated TOP2A, TOP2B, and ZATT/ZNF451 may indicate an anticipated role of RAD54L2 in the regulation of TOP2A, TOP2B, and ZATT/ZNF451 functions and/or the removal of TOP2ccs.

RAD54L2 reduces chromatin-bound TOP2 with or without ETO treatment and this function requires its ATPase activity

To understand how RAD54L2 regulates the functions of TOP2A, TOP2B, and ZATT/ZNF451 especially after treatment with TOP2 poison, we analyzed the consequence of mutating the ATPase activity of RAD54L2. It is known that SNF2 family proteins function as chromatin remodelers driven by ATP hydrolysis (*26*, *42*). Given the key functions of ATPase activity in SNF2 family proteins, we generated an ATPase-defective mutant of RAD54L2, i.e., RAD54L2^{K310A}, and showed that RAD54L2^{K310A} could not rescue ETO sensitivity caused by RAD54L2 loss in control cells or in cells with TDP2 loss (Fig. 5, A and B). However, RAD54L2^{K310A} could still be detected in the proximity of TOP2A (fig. S7A). Thus, RAD54L2′s function requires its ATPase activity.

As SNF2 family translocases are known to displace proteins from DNA (*42*), we then checked whether the ATP hydrolysis driven by RAD54L2 would affect the chromatin association of TOP2A, TOP2B, and ZATT/ZNF451. We quantified the chromatin-bound TOP2A/TOP2B using TurboNuclease-mediated chromatin purification. While depletion of RAD54L2 did not change the amount of TOP2A/TOP2B in whole-cell extracts (WCE) (Fig. 5C, left), the chromatin-bound TOP2A/TOP2B increased in RAD54L2-KO cells even without ETO treatment (Fig. 5, C, right, and D). The TurboNuclease-mediated chromatin purification assay cannot distinguish covalently bound or noncovalently bound TOP2 on chromatin. To exam whether the excess binding of TOP2A/TOP2B on chromatin in RAD54L2-KO cells increase the chance of TOP2A/TOP2B to be trapped by ETO, we examined TOP2ccs trapping using a DUST (detection of ubiquitylated and SUMOylated TOP-DPC) assay (*11*). RAD54L2 loss caused accumulation of total TOP2Accs on DNA following ETO treatment (Fig. 5E and fig. S7B). Pretreatment with proteasome inhibitor MG132 also caused an accumulation of TOP2Accs (Fig. 5E and fig. S7B). Simultaneous depletion of RAD54L2 and inhibition of proteasome activity has a slightly additive effect on the accumulation of total TOP2Acc (Fig. 5E and fig. S7B). Together, our results lead to the conclusion that RAD54L2 prevents excess chromatin binding of TOP2A/TOP2B with or without ETO treatment. We also observed a higher SUMO-2/3 modification on the accumulated TOP2ccs with RAD54L2 loss (Fig. 5E and fig. S7C), suggesting that RAD54L2 potentially accounts for the removal of SUMOylated TOP2A/TOP2B from chromatin.

The data shown above suggest that loss of RAD54L2 increases the chromatin binding of TOP2A/TOP2B, which enhances the chance of TOP2A/TOP2B to be trapped by ETO. To understand the mechanisms underlying how RAD54L2 loss would lead to increased chromatin binding of TOP2, we used purified RAD54L2 protein to perform in vitro biochemical assays. ETO treatment stabilized the formation of TOP2Acc in vitro and led to the accumulation of intermediate linear DNA (Fig. 5F, lane 3). Addition of RAD54L2 reduced the amount of ETO induced TOP2Acc without changing the amount of linear DNA (Fig. 5F, lane 4).

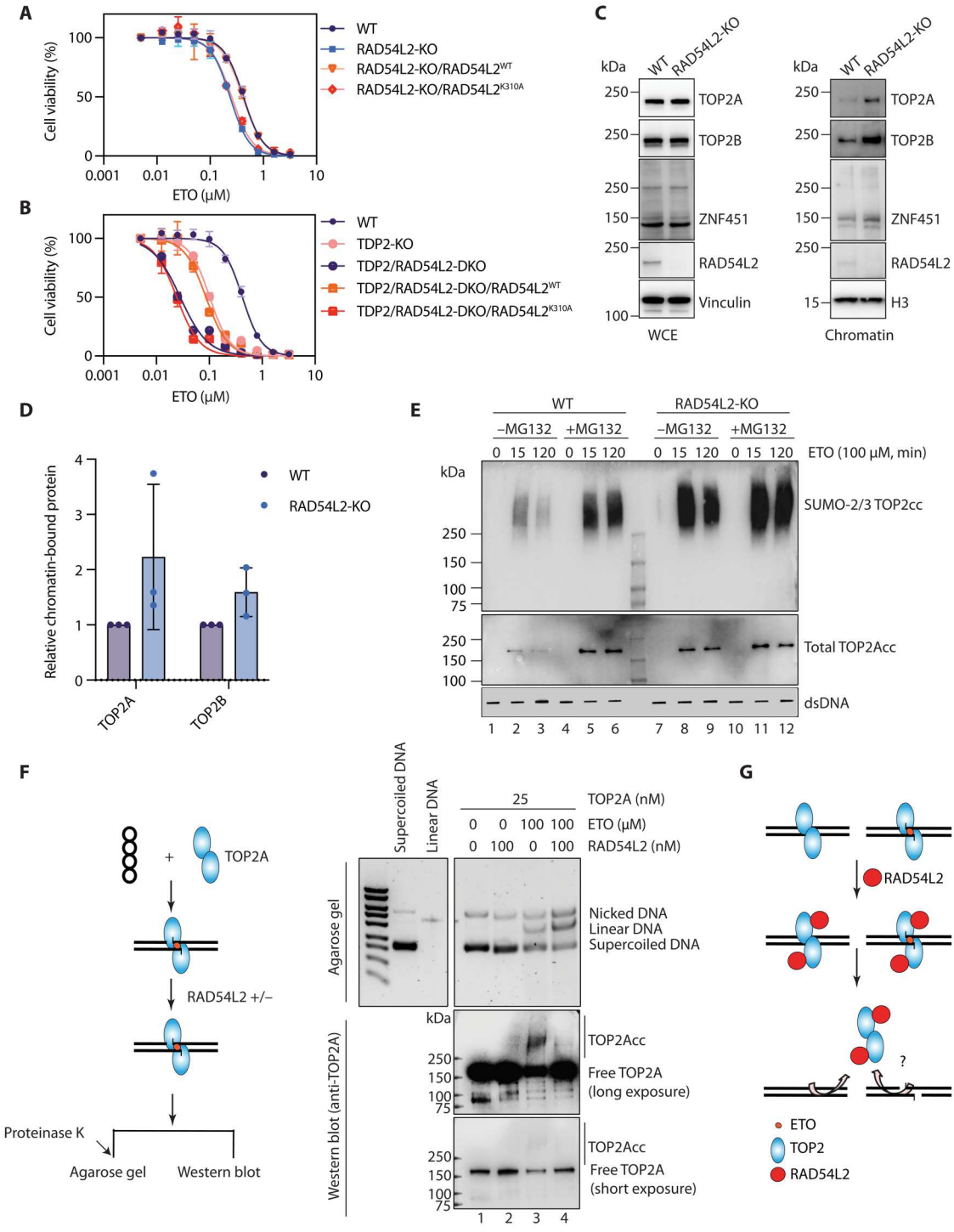

Fig. 5. RAD54L2 reduces chromatin-bound TOP2 with or without ETO treatment, and this function requires its ATPase activity. (**A**) RAD54L2-KO cells were infected with virus expressing RAD54L2^{WT}-SFB or RAD54L2^{K310A}-SFB. Cell proliferation was measured using a CellTiter-Glo assay after 4 days in the presence of the indicated concentrations of ETO. Data are presented as the mean ± SD (n = 3). (**B**) TDP2/RAD54L2-DKO cells were infected with virus expressing RAD54L2^{WT}-SFB or RAD54L2^{K310A}-SFB. Cell proliferation was measured using a CellTiter-Glo assay after 4 days in the presence of the indicated concentrations of ETO. Data are presented as the mean ± SD (n = 3). (**C**) WCE and TurboNuclease-mediated chromatin fraction of WT and RAD54L2-KO cells were prepared and subjected to Western blotting with the indicated antibodies. (**D**) Quantification of (C) from three independent experiments. Mean ± SD are shown. (**E**) WT and RAD54L2-KO cells were pretreated with 10 μM MG132 for 1 hour and then treated with 100 μM ETO for indicated times. Samples were collected for DUST assay to detect SUMO-2/3, and total TOP2A-DPCs. dsDNA is used as a loading control. dsDNA was run at the same gel but cut for presentation as shown. (**F**) In vitro TOP2 cleavage assay was performed with indicated amounts of proteins. Reactions were conducted at 37°C for 20 min. Western blotting was conducted for the detection of TOP2Acc and free TOP2A with anti-TOP2A antibody. Proteinase K was used to digest all proteins before running agarose gel. (**G**) A model showing that RAD54L2 prevents the excessive accumulation of TOP2 on chromatin with or without ETO treatment.

Linear DNA is an intermediate of the TOP2 cleavage cycle, which is undetectable under normal conditions (Fig. 5F, lanes 1 and 2). ETO treatment inhibited the resealing of transiently formed TOP2cc, which leads to stabilized TOP2cc with linear DNA. Thus, formation of linear DNA represents started but not finished TOP2 cleavage cycles. The remaining linear DNA in lane 4 indicates a role of RAD54L2 in direct removal of trapped TOP2Acc. However, it remains to be determined whether such reaction truly occurs in vivo, because the in vitro experiments were performed with high concentrations of RAD54L2, TOP2A, and ETO. In a rare situation that RAD54L2 removes trapped TOP2 directly, we suspect that the remaining unsealed DNA ends can be easily rejoined by NHEJ or other strand break repair pathways.

We also monitored how RAD54L2 affects the activity of TOP2A. We found that addition of RAD54L2 compromised the decatenation activity of TOP2A toward Kinetoplast DNA (kDNA) (fig. S8, A and B), probably due to the removal of TOP2A from DNA by RAD54L2. We observed a reduction, but not absence, of the ATPase mutant of RAD54L2 on the inhibition of TOP2A activity and removal of TOP2Acc (fig. S8, A to C). We speculate that the point mutant of RAD54L2 may still retain some ATPase activity and function in vitro, but it cannot rescue ETO sensitivity due to RAD54L2 loss in cells. Together, we hypothesize that RAD54L2 alleviates the genotoxic effect of ETO treatment by both preventing the excessive accumulation of TOP2 on chromatin and possibly disrupting TOP2cc after treatment with TOP2 poison (Fig. 5G).

Chromatin association of RAD54L2 depends on its interaction with SUMOylated proteins

As mentioned at the beginning, it was proposed that suppression of proteasome-mediated processing of TOP2ccs would enhance TOP2ccs reversal and promote the removal of intact TOP2 from chromatin (*7*). We speculated a role of RAD54L2 in removing TOP2 and possibly trapped TOP2ccs from chromatin above. Therefore, we checked whether there is any relationship between RAD54L2 and the proteasome-mediated processing of TOP2ccs. We pre-extracted cells with Triton before fixation to check the chromatin-bound proteins by immunofluorescence staining. We found that inhibition of the proteasome by MG132 notably enhanced the chromatin association of RAD54L2 (Fig. 6A), without changing its WCE expression level (fig. S9A). The global interaction between RAD54L2 and TOP2A was not notably changed upon MG132 treatment (Fig. 4C and fig. S9B). However, when we used PLA to monitor the interaction between chromatin-bound RAD54L2 and TOP2A, we observed an increase of this interaction after MG132 treatment (fig. S9B). Accordingly, upon MG132 treatment we observed increased RAD54L2 chromatin loading and a reduction of chromatin-bound TOP2A/TOP2B (Fig. 6B and fig. S9C), probably due to the proposed role of RAD54L2 in the removal of TOP2 from DNA. Please note that MG132 treatment not only inhibits the proteasome activity but also depletes free ubiquitin globally (*43*, *44*). Thus, it is possible that the proteasome- and/or ubiquitin-dependent events are involved in the dynamic regulation of RAD54L2 chromatin association, which requires further investigation.

Nevertheless, we found that combined treatment of MG132 with SUMOylation inhibitor ML-792 abolished enhanced chromatin binding of RAD54L2 caused by MG132 treatment alone (Fig. 6A). ML-792 treatment abolished the interaction of RAD54L2 with SUMOylated proteins (Fig. 4C). Treatment of ML792 also reduced the enhanced chromatin binding of RAD54L2 caused by MG132 treatment alone in TurboNuclease-mediated chromatin purification assay (Fig. 6B). These data suggest that the binding to SUMOylated proteins is critical for RAD54L2 chromatin recruitment and/or retention.

RAD54L2, ZATT/ZNF451 and TDP2 represent overlapping pathways involved in the regulation of TOP2 and TOP2cc removal

ZATT/ZNF451 is a well-known SUMO E3 ligase of TOP2A/TOP2B (*13*, *33*). It interacts with TOP2A/TOP2B with or without DNA damage and SUMOylates TOP2A/TOP2B (*13*). We showed that RAD54L2 also interacted with ZATT/ZNF451 (Fig. 3, A, B, and F). We first checked whether deletion of RAD54L2 would affect the interaction between TOP2A and ZATT/ZNF451. Results showed that ZATT/ZNF451 interacted with TOP2A with or without RAD54L2 (fig. S10A). To check whether there is any functional interaction between RAD54L2 and ZATT/ZNF451, we assayed the genetic interaction between RAD54L2 and ZATT/ZNF451 by knocking down ZATT/ZNF451 in both WT and RAD54L2-KO cells. In agreement with previous findings (*13*, *29*), knockdown of ZATT/ZNF451 in WT cells conferred hypersensitivity to ETO treatment (Fig. 6, C and D). Similar results were obtained with knockout of ZATT/ZNF451 (fig. S10, B and C). However, we noticed that ZATT/ZNF451-KO cells gradually lost their severe ETO sensitivity after proliferating for several generations, which was accompanied by increased growth rate and changed morphology. We speculated that ZATT/ZNF451 depletion may cause such a high burden to cell survival due to inefficient resolution of TOP2-linked DNA damage, for which cells have to rely on other mechanisms to maintain cell proliferation. Thus, we only present the results obtained with immediate knocking down or knockout of ZATT/ZNF451. We found that codeficiency of RAD54L2 and ZATT/ZNF451 had a comparable sensitivity to ZATT/ZNF451 single deficiency (Fig. 6, C and D, and fig. S10, B and C), indicating that RAD54L2 is epistatic to ZATT/ZNF451.

Next, we used a DUST assay to monitor the removal of TOP2cc (*11*). Overexpression of RAD54L2 in both WT and RAD54L2-KO cells facilitated the removal of TOP2Acc (Fig. 6E and fig. S10D). Further knocking down of ZATT/ZNF451 reversed the effect caused by RAD54L2 overexpression and led to more TOP2Acc accumulation (Fig. 6E and fig. S10D). These results agree with previous findings (*13*, *29*) that ZATT/ZNF451 plays a critical role in the removal of TOP2ccs and further demonstrate the epistatic relationship between ZATT/ZNF451 and RAD54L2. We also observed that deficiency of ZATT/ZNF451 led to reduced SUMO-2/3 modified TOP2ccs (Fig. 6E and fig. S10E), revealing a key function of ZATT/ZNF451 in SUMOylating TOP2ccs (*13*).

ZATT/ZNF451 is known to facilitate TDP2-mediated cleavage of TOP2ccs (*13*). However, it has also been suggested to operate through TDP2-independent mechanisms in cellular response to TOP2-induced damage (*13*, *29*). In addition, ZATT/ZNF451 has been suggested to mediate SUMOylation of TOP2A in response to replication stress (*34*). To determine whether RAD54L2 accounts for the TDP2-independent function of ZATT/ZNF451 in response to TOP2-induced damage, we generated ZATT/ZNF451- and RAD54L2-deficient cells in the background of TDP2 loss. We found that in the background of TDP2 loss, depletion of RAD54L2 caused similar ETO sensitivity comparing to knocking

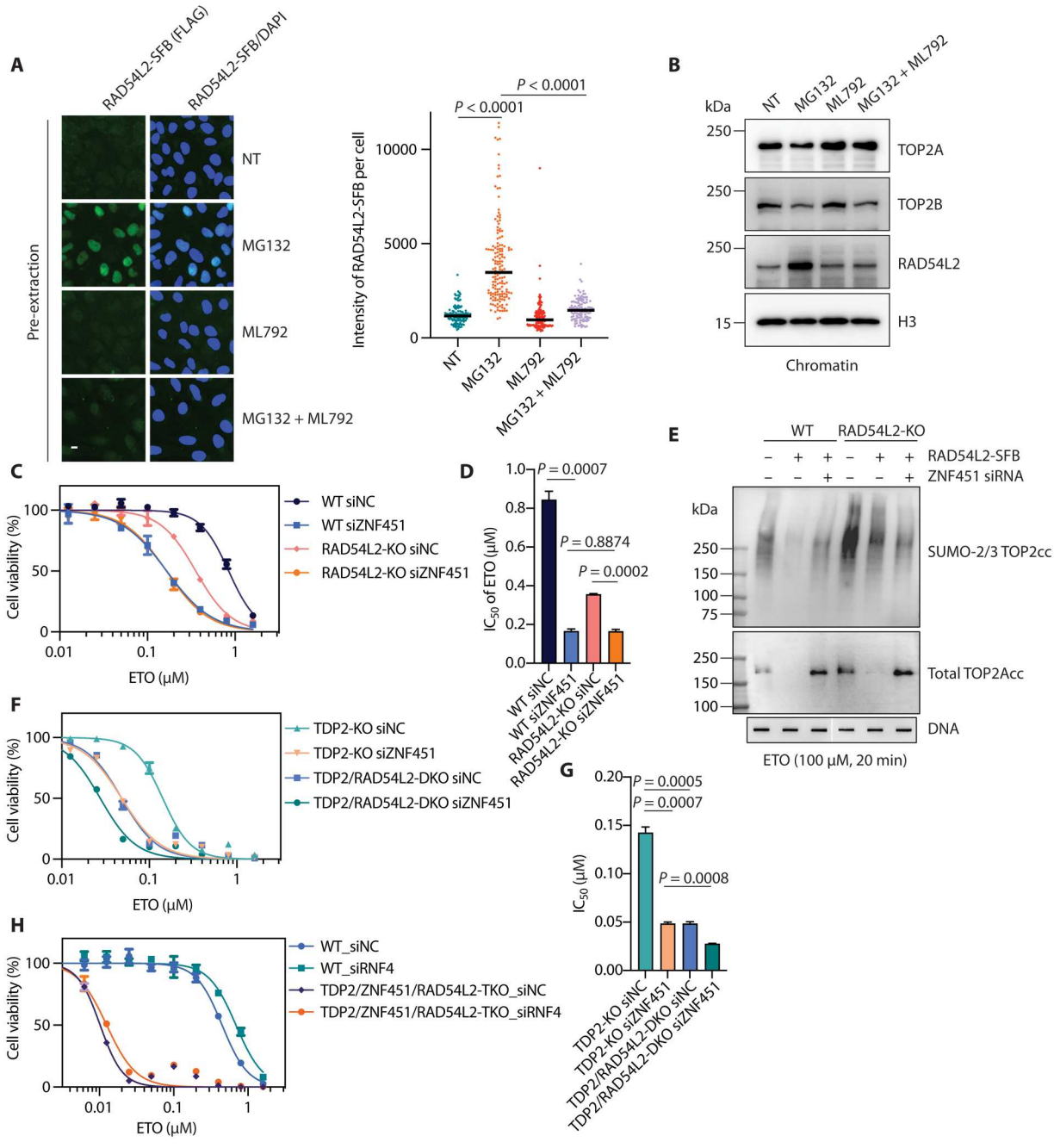

Fig. 6. RAD54L2, ZNF451, and TDP2 constitute overlapping pathways involved in cellular resistance to ETO. (**A**) Representative images of RAD54L2-SFB localization to chromatin with the indicated treatment are presented. Scale bar, 10 μm. Quantification of RAD54L2-SFB intensity per cell were shown. The median intensity was indicated. (**B**) Chromatin association of indicated proteins were determined with Western blotting with indicated treatment. Histone H3 served as loading control. (**C**) WT and RAD54L2-KO cells were transfected with siNC (nontargeting control) or siRNAs targeting ZNF451. Cell proliferation was measured using a CellTiter-Glo assay after 4 days in the presence of the indicated concentrations of ETO. Data are presented as the mean ± SD ($n = 3$). (**D**) A two-tailed unpaired *t* test was used for statistical analysis of the IC50 of ETO treatment of each cell line in (C). (**E**) WT and RAD54L2-KO cells were transfected with constructs encoding RAD54L2-SFB or infected with siRNAs targeting ZNF451. Cells were treated with 100 μM ETO for 20 min. Samples were collected for DUST assay to detect SUMO-2/3, and total TOP2-DPCs. dsDNA is used as a loading control. (**F**) TDP2-KO and TDP2/RAD54L2-DKO cells were transfected with siNC or siRNAs targeting ZNF451. Cell proliferation was measured using a CellTiter-Glo assay after 4 days in the presence of the indicated concentrations of ETO. Data are presented as the mean ± SD ($n = 3$). (**G**) A two-tailed unpaired *t* test was used for statistical analysis of the median inhibitory concentration (IC_{50}) of ETO treatment of each cell line in (F). (**H**) WT and TDP2/ZNF451/RAD54L2-TKO cells were transfected with siNC or siRNAs targeting RNF4. Cell proliferation was measured using a CellTiter-Glo assay after 4 days in the presence of the indicated concentrations of ETO. Data are presented as the mean ± SD ($n = 3$).

down or knocking out of ZATT/ZNF451 (comparing TDP2-KO siZNF451 and TDP2/RAD54L2-DKO siNC) (Fig. 6, F and G, and fig. S10, F and G), which agree with our hypothesis. However, we found that depletion of ZATT/ZNF451 in TDP2/RAD54L2-DKO cells and depletion of RAD54L2 in TDP2/ZNF451-DKO cells made cells slightly more sensitive to ETO treatment (Fig. 6, F and G, and fig. S10, F and G), suggesting that ZATT/ZNF451 and RAD54L2 may have largely overlapping but not identical functions. This genetic interaction data suggest that RAD54L2, ZATT/ZNF451, and TDP2 have both redundant and separated functions.

We noticed that while loss of ZATT/ZNF451 slowed down cell growth, depletion of TDP2 or RAD54L2 did not cause any notably defect in cell proliferation, which suggests that ZATT/ZNF451-dependent pathways are likely to be more important for TOP2 removal in untreated cells. In agreement, loss of ZATT/ZNF451 caused a higher sensitivity to ETO than depletion of RAD54L2 or TDP2 (fig. S11, A and B). Depletion of TDP2 caused less sensitivity to ETO than ZNF451 loss, but more than that of RAD54L2 loss (fig. S11, A and B). TDP2 not only functions with ZATT/ZNF451 to remove SUMOylated TOP2ccs (*13*) but also can hydrolyze the residue peptides after proteosome-mediated degradation of TOP2ccs (*12*). Depletion of RAD54L2 caused relative mild sensitivity than TDP2 or ZATT/ZNF451 loss (fig. S11, A and B). Moreover, we did not observe any obvious difference in cell proliferation in untreated conditions when overexpressing RAD54L2. However, we did notice some mild resistance to ETO treatment after RAD54L2 overexpression (fig. S11C), which is in consistence with our findings in Fig. 6E. As mentioned above, the mild phenotypes observed in cells with RAD54L2 depletion or overexpression are likely due to additional regulation of TOP2 homeostasis by ZATT/ZNF451. Overexpression of ZNF451 was toxic to cells and knockout of ZNF451 also caused burden to cell proliferation.

We then examined the effect of RNF4 depletion with the deficiency of RAD54L2, ZATT/ZNF451, and TDP2. We found that knocking down of RNF4 in TDP2/ZNF451/RAD54L2 TKO cells still led to some resistance to ETO (Fig. 6H), indicating that besides the functions of TDP2, ZATT/ZNF451, and RAD54L2 in the removal of trapped TOP2cc, there might be other mechanisms that promote cell survival when proteasome-mediated processing of TOP2ccs is suppressed.

DISCUSSION

In this study, we describe a RAD54L2-mediated pathway that prevents excess binding of TOP2 on chromatin and reduces trapped TOP2ccs formed in response to TOP2 poison treatment. We hypothesize that this dynamic regulation of TOP2 by RAD54L2 represents an intrinsic TOP2-specific DNA damage avoidance pathway to reduce potential DNA damage mediated by TOP2. Similar mechanism was previously reported in yeast (*45*). Rrp2, which also belongs to SWI2/SNF2-family (*46*, *47*), was shown to be critical for cellular resistance to Top2 poison in fission yeast (*45*). It was demonstrated that Rrp2 interacts with SUMOylated Top2 through its SUMO-interaction motifs, which protects Top2-SUMO from being ubiquitinated by STUbLs Rfp1-Slx8 (ortholog of RNF4) and degraded presumably by the proteasome (*45*). This active

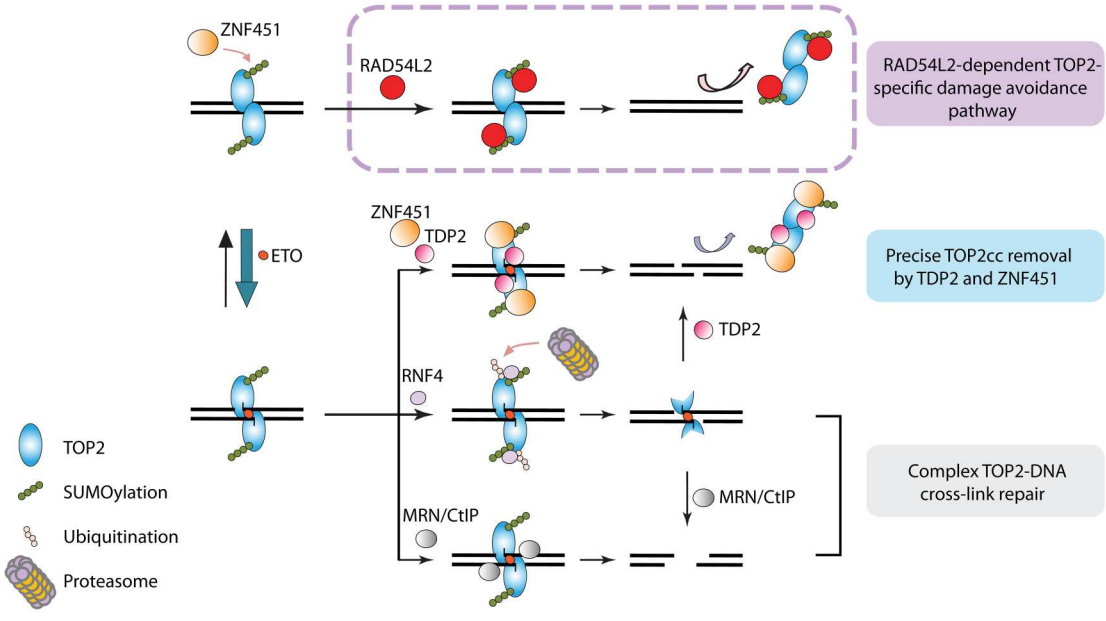

Fig. 7. A model of multiple mechanisms involved in the resolution of TOP2 and TOP2-linked DNA damage. TOP2 forms transient TOP2cc during its catalytic cycle, which can be trapped by TOP2 poisons such as ETO. Here, we propose that RAD54L2 directly remove excess TOP2 on chromatin and thus reduce TOP2cc formation, especially when cells are treated with TOP2 poisons. This conserved RAD54L2-dependent TOP2-specific DNA damage avoidance pathway acts to ensure genome stability. Once the trapped TOP2cc forms, it can also be resolved via several distinct mechanisms. First, it can be precisely removed by the coordinated actions of TDP2 and ZATT/ZNF45. Second, TOP2cc can be targeted by RNF4-mediated pathway for ubiquitination and degradation. Residual peptides after proteasome-mediated degradation can be further processed by TDP2 or other repair enzymes such as MRN/CtIP. Third, MRN/CtIP or other repair enzymes can cleave the DNA strands in the vicinity of intact trapped TOP2cc or proteolytically processed TOP2cc with residual peptides. The RNF4/proteasome-mediated and/or MRN/CtIP-dependent processing of TOP2cc lead to more complex DNA repair events and activate DNA damage responses.

prevention of Top2 degradation also led to the avoidance of exposure of concealed DNA breaks (*45*). Similarly to RAD54L2, the ATPase activity of Rrp2 is required for the displacement of Top2 from DNA (*45*). Uls1, the ortholog of Rrp2 in budding yeast, was also shown to function in protecting the genome from Top2 poisons (*45*). The similarity between RAD54L2 and yeast Rrp2/Uls1 suggests a conserved mechanism that tightly regulates TOP2 on chromatin, thus specifically avoiding the formation of unwanted TOP2-linked DNA damage. The existence of this conserved TOP2-specific damage avoidance pathway highlights the delicate balance between the critical functions of TOP2 in key cellular processes and the importance of genome maintenance in cell proliferation and survival.

Of course, there are also some differences between yeast and human proteins. For example, it was shown that loss of Rrp2 enhanced SUMOylation-dependent ubiquitination and degradation of Top2, but such excessive degradation of TOP2 by proteasomal activity was not observed in our study in cells with RAD54L2 loss. While it is likely that RAD54L2, similar to yeast Rrp2, may compete with RNF4 for the binding to SUMOylated TOP2, the situation in humans is more complex. We speculate that this may be due to additional regulations that exist specifically in human cells, which are not present in yeast. For example, besides the RAD54L2-dependent TOP2-specific damage avoidance pathway described here, the removal of TOP2ccs involves several other mechanisms (Fig. 7). ZATT/ZNF451-mediated TDP2-dependent pathway can also remove SUMOylated TOP2ccs by precisely hydrolyzing the covalent bonds between TOP2 and DNA (*13*). ZATT/ZNF451 is a vertebrate-specific SUMO E3 ligase that no ortholog has been identified in yeast yet. In addition, there is also no TDP2 ortholog in yeast, making the ZATT/ZNF451-mediated TDP2 pathway unique in human cells.

Besides the RAD54L2-dependent damage avoidance pathway and ZATT/ZNF451 and TDP2-dependent TOP2cc precision repair pathway, trapped TOP2ccs can be also targeted by RNF4-mediated pathway for ubiquitination and proteasomal degradation in higher eukaryotes (Fig. 7) (*7*, *11*). How the proteasome-mediated pathway coordinates with ZATT/ZNF451-TDP2– and RAD54L2-mediated TOP2cc removal remains unclear. As mentioned above, we speculate that RNF4/proteasome pathway may compete with ZATT/ZNF451-TDP2 and RAD54L2 pathways for SUMOylated TOP2ccs substrate. Following the proteolytic degradation of TOP2ccs, small peptide residues are left, which must be processed by TDP2 or other repair enzymes such as MRN/CtIP (*19*). TDP2-dependent hydrolysis results in a protein/peptide-free DSB that can be ligated by NHEJ without further nucleolytic processing, providing a direct mechanism for DSB repair. Nucleases like MRN/CtIP can cleave DNA strands in the vicinity of either an intact trapped TOP2cc or proteolytic degraded TOP2cc (*14*–*19*), which generates DSB that can be further repaired by HR or NHEJ, which is potentially mutagenic. As previously reported (*7*), RNF4 and proteasome processing of TOP2ccs would lead to irreversible DPC formation, activate DNA damage responsive pathway, and result in cytotoxic and genome instability due to error-prone repair of these TOP2ccs intermediates.

As the evolutionally conserved pathway, RAD54L2 regulates TOP2 homeostasis and remove SUMOylated TOP2 from chromatin, which reduce the possibility of trapped TOP2 intermediates, and thus decreases the amount of TOP2ccs formed at the beginning and avoids proteasome-mediated degradation of TOP2ccs. ZATT/ZNF451 binds tightly to TOP2A/TOP2B and SUMOylates TOP2A/TOP2B in response to ETO treatment or replication stress (*13*, *34*). The ZATT/ZNF451 may be the key factor in humans because it promotes not only the RAD54L2-dependent DNA damage avoidance pathway but also the precision repair of TOP2ccs through ZATT/ZNF451-TDP2-dependent error-free pathway. The multiple mechanisms involved in TOP2cc removal summarized in Fig. 7 underscore the critical functions and regulations of TOP2 in humans.

MATERIALS AND METHODS

Cells and cell culture

HeLa and HEK293T cells were purchased from the American Type Culture Collection (ATCC) (Manassas, VA) and maintained in Dulbecco's modified Eagle's medium containing 10% fetal calf serum at 37°C with 5% CO_2. HEK293A cells were purchased from Thermo Fisher Scientific (R70507) and maintained in Dulbecco's modified Eagle's medium containing 10% fetal calf serum at 37°C with 5% CO_2. U2OS cells were purchased from the ATCC (Manassas, VA) and maintained in McCoy's 5A (Modified) medium containing 10% fetal calf serum at 37°C with 5% CO_2.

Knockout cell lines were generated using lentiCRISPR v2 (52961; Addgene) as previously described (*28*, *48*). In brief, single guide RNAs (sgRNAs) targeting specific genes were cloned into lentiCRISPR v2. Then, lentiCRISPR v2-sgRNA plasmids were transfected into HEK293A or HeLa cells, using X-tremeGENE HP DNA Transfection Reagent (06366546001; Sigma-Aldrich). Twenty-four hours after transfection, cells were treated with puromycin for another 2 days and were then seeded into 96-well plates for single-clone formation. Two weeks after seeding, single clones were picked and examined by Western blotting to determine the expression of the targeted gene. The sgRNAs used in this study were (i) TDP2: TCTCCCAGTCGTTCTCGGCC, (ii) ZATT/ZNF451: T GTTCTTGAATACATTGATC, (iii) RAD54L2-2: GGGTAATACT GCGCATACGA, (iv) RAD54L2-T2: GTATACCCGACATACTGC CT, and (v) RAD54L2-T4: CATTGAGTACTGGTGCATGG.

For the generation of U2OS RAD54L2^{WT}-SFB and U2OS RAD54L2^{K310A}-SFB stable cell lines, U2OS cells were infected with either pLEX_307-SFB control virus, generated from pLEX_307 (41392; Addgene) by X.F., pLEX_307-RAD54L2^{WT}-SFB virus, or RAD54L2^{K310A}-SFB virus. After infection, cells were selected with puromycin for 7 days to get pooled RAD54L2 stable expression cells. Single clones were selected to detect the expression level of RAD54L2. Clones with similar levels of RAD54L2^{WT}-SFB and RAD54L2^{K310A}-SFB were chosen for further analysis. cDNA of RAD54L2^{WT} was purchased from OriGene Technologies (RC206881). RAD54L2^{K310A} was generated by polymerase chain reaction (PCR)–mediated site-directed mutagenesis and verified by sequencing.

Antibodies, chemicals, and siRNAs

In this study, antibodies used for Western blotting or slot blotting included RAD54L2 (ab86063; Abcam), TOP2A (ab52934; Abcam), TOP2B (A300-950A; Bethyl Laboratories), ZATT/ZNF451 (NBP2-94743; Novus Biologicals), SUMO-2/3 (4971S; Cell Signaling Technology), SUMO-1 (4940S; Cell Signaling Technology), FLAG (F3165; Sigma-Aldrich), RNF4 (AF7964-100; R&D Systems), double-stranded DNA (dsDNA) (ab27156; Abcam), phospho-DNA-PKcs (S2056, ab18192; Abcam), phospho-KAP1 (S824,

4127S; Cell Signaling Technology), phospho-ATM (S1981, ab81292; Abcam), phospho-Chk2 (Thr68, 2661S; Cell Signaling Technology), phospho-H2AX (S139, 9718S; Cell Signaling Technology), phospho-RPA32 (S4/S8, A300-245A; Bethyl Laboratories), TDP2 (sc-377280; Santa Cruz Biotechnology), H3 (ab1791; Abcam), RAD51 (ab63801; Abcam), tubulin (T6199-200UL; Sigma-Aldrich), and vinculin (V9131; Sigma-Aldrich).

Antibodies used for FACS analyses included phospho-H2AX (S139, 05-636 l; Millipore) and Alexa Fluor Plus 488 (A32723; Thermo Fisher Scientific). Antibodies used for immunofluorescence staining of PLAs and pre-extraction experiments included TOP2A (ab52934; Abcam), ZATT/ZNF451 (NBP2-94743; Novus Biologicals), FLAG (F3165; Sigma-Aldrich), and phospho-H2AX (S139, 9718S; Cell Signaling Technology).

The chemicals used in this study included ETO (E1383100MG; Thermo Fisher Scientific), MG132 (S2619; Selleck Chemicals), ML-792 (HY-108702; MedChem Express), doxorubicin (S1208; Selleck Chemicals), CPT (390238-25MG; Calbiochem), cisplatin (S1166; Selleck Chemicals), HU (H8627-10G; Sigma-Aldrich), pyridostatin (S7444; Selleck Chemicals), and ICRF-187 (S1222; Selleck Chemicals).

ON-TARGETplus human siRNA smart pool for RNF4 (L-006557-00-0005), ZATT/ZNF451 (L-013935-01-0005), RAD54L2 (L-014122-01-0005), RAD51 (L-003530-00-0005), and ON-TARGETplus nontargeting siRNA (D-001810-01-20) were purchased from Dharmacon. siRNA transfections were performed using Lipofectamine RNAiMAX Transfection Reagent (13778075; Thermo Fisher Scientific) following manufacturer's instructions. All siRNAs were used at a final concentration of 50 nM.

CellTiter-Glo assay

Cell viability was measured by CellTiter-Glo assay using CellTiter-Glo (G7572; Promega, Madison, WI) reagents. In brief, diluted cells (1000 cells in 100 μl) were seeded onto 96-well plates. One day after seeding, 10 μl of serially diluted concentrations of indicated chemicals was added into each well. For infrared treatment, cells were irradiated directly on the plate. Cells were then incubated for another 4 days in the presence of indicated chemicals. Cell viability was measured as previously described (*28*).

Colony formation assay

For analysis of cell viability using colony formation assay, HEK293A WT and TDP2-KO cells were transfected with siNC (nontargeting control) or siRNAs targeting RNF4. One day after transfection, cells were diluted and seeded in six-well plates (100 cells for NT, 400 cells for 0.1 μM ETO, and 1600 cells for 0.2 μM ETO). One day after seeding, cells were treated with indicated concentrations of ETO for 24 hours. Cells were then incubated for another 10 days before crystal violet staining and visualization. Plates were scanned by a ChemiDoc imaging system (Bio-Rad). Cell colonies were analyzed using ImageJ software (version 1.50i).

Whole-genome CRISPR-Cas9 screening

Whole-genome CRISPR-Cas9 screening was conducted as described previously using TKOv3 gRNA library (*28*, *29*). In brief, HEK293A WT and TDP2-KO cells were infected with lentiviruses packaged from the TKOv3 library at a low multiplicity of infection (<0.3). Twenty-four hours after infection, infected cells were selected with puromycin for 2 days. The remaining cells after selection were divided into two different treatment groups: the not-treated (NT) and ETO-treated groups with three replicates in each group. Cells were then subcultured every 3 days, with a total of 21 days. The day after selection was set as day 0 (T0). Part of cells from T0 and T21 were collected for genomic DNA extraction using a QIAamp Blood Maxi Kit (QIAGEN). gRNAs that inserted into the genome were amplified via PCR using primers harboring Illumina TruSeq adapters with i5 and i7 barcodes, as described previously (*28*). The resulting PCR products were purified and sequenced using an Illumina HiSeq 2500 system. Data analyses were performed with a MAGeCK (https://sourceforge.net/p/mageck/wiki/Home/) (*30*) and drug Z (https://github.com/hart-lab/drugz, version 1.1.0.2) (*31*). ETO sensitivity profiling was analyzed by comparing the differences in gRNA abundance between ETO-treated group and NT group in each cell line using drug Z.

FACS analyses

HEK293A WT, RAD54L2-KO, TDP2-KO, and TDP2/RAD54L2-DKO cells were either not-treated (NT) or treated with 4 μM ETO for 2 hours or 1 μM ETO for 1 hour as indicated in the figure legends. Cells were then collected and fixed with ice-cold 70% ethanol at 4°C overnight. After fixation, cells were permeabilized with 0.5% Triton X-100/ phosphate-buffered saline (PBS) for 10 min and blocked with 4% bovine serum albumin (BSA)/PBS for 1 hour at room temperature. Cells were then incubated with phospho-H2AX (S139, 05-636 l; Millipore) diluted in 4% BSA/PBS at 4°C overnight. At the following day, cells were then incubated with Alexa Fluor Plus 488 (A32723; Thermo Fisher Scientific) for 1 hour at room temperature in the dark. FxCycle Violet Satin (F10347; Thermo Fisher Scientific) was added before cells were analyzed with Attune Flow cytometers (Thermo Fisher Scientific). Data were analyzed with FlowJo software (FlowJo 10.6.1, Becton Dickinson).

DSB-induced HR repair reporter assay

U2OS cells stably expressing HR repair DR-GFP reporter were transfected with nontargeting siRNA, siRNA targeting RAD54L2, and/or siRNA targeting RAD51. Twenty-four hours after transfection, 2 μg of I–Sce I expression vector or control vector was transfected into the cells using Lipofectamine 3000 Transfection Reagent (L3000015; Thermo Fisher Scientific). Cells were then collected 48 hours later and subjected to FACS analysis to determine the proportion of GFP-positive cells.

DUST assay

DUST assay was used to detect the accumulation of covalently bound TOP2 on chromatin (*11*). The assay was performed as described previously (*11*). In brief, 1 million cells were subjected to indicated drug treatment. Cells were then lysed with 600 μl of DNAzol (Invitrogen). Three hundred microliters of 200 proof ethanol was added to precipitate the nucleic acids. The collected nucleic acids were then washed with 75% ethanol and resuspended in 200 μl of tris-EDTA (TE) buffer. The resuspended sample was heated at 65°C for 15 min and sheared with sonication (40% output for 10-s pulse and 10-s rest for four times). The supernatant was harvested after centrifugation and treated with RNase A (100 μg/ml) for 1 hour at 4°C. The sample was then precipitated with 1:10 volume of 3 M sodium acetate and 2.5 volume of 200-proof ethanol. DNA pellet collected after centrifugation was resuspended

in 100 μl of TE buffer. DNA concentration was determined by NanoDrop. DNA (10 μg) from each sample was then digested with 50 U of micrococcal nuclease (100 U/μl; Thermo Fisher Scientific) in the presence of 5 mM $CaCl_2$. After digestion, samples were subjected to electrophoresis on 4 to 15% precast polyacrylamide gel (Bio-Rad) for immunodetection of total TOP2cc, SUMOylated TOP2cc, and ubiquitylated TOP2cc using specific antibodies. At the same time, 2 μg of each sample was subjected to slot blot for immunoblotting with anti-dsDNA antibody as a loading control.

WCE preparation and chromatin purification

For WCE preparation, cells were washed with PBS and then resuspended in 1× Laemmli buffer for cell lysis. The cell lysate was then boiled at 95°C for 10 min and subjected to Western blotting.

For chromatin purification, 2 million cells were washed with PBS and resuspended in 1 ml of ice-cold NETN buffer [50 mM tris-HCl (pH 7.4), 100 mM NaCl, 0.4% NP-40, 1 mM EDTA, protease inhibitor cocktail, and 20 mM *N*-ethylmaleimide]. The cell lysates were rotated at 4°C for 10 min to induce adequate cell lysis. Samples were then centrifugated, and pellets were collected. The harvested pellets were washed with 1 ml of NETN buffer and then 1 ml of TurboNuclease buffer [50 mM tris-HCl (pH 8.0), 150 mM NaCl, 2 mM $MgCl_2$, protease inhibitor cocktail, and 20 mM *N*-ethylmaleimide] separately. TurboNuclease buffer (200 μl) supplemented with 250 U of TurboNuclease enzyme (9207-50KU; VWR) was then added to resuspend the pellets. The resuspended samples were then incubated at 4°C for 1 hour. Supernatants were then collected after centrifugation and diluted with 4× Laemmli buffer. Samples were boiled at 95°C for 10 min and subjected to Western blotting.

Immunoprecipitation

HEK293A WT cells were either transfected with constructs encoding SFB-tagged proteins or empty vector as control using X-tremeGENE HP DNA Transfection Reagent (06366546001; Sigma-Aldrich). Twenty-four hours after transfection, cells were treated with indicated chemicals and subjected to immunoprecipitation. Briefly, cells were lysed in ice-cold NETN buffer for 10 min at 4°C. The supernatant was then collected after centrifugation and mixed with S beads for 3 hours at 4°C with rotation. After incubation, the beads were then washed three times with NETN buffer before elution with 2× Laemmli buffer.

Immunofluorescence staining

U2OS RAD54L2^{WT}-SFB and U2OS RAD54L2^{K310A}-SFB stable expression cell lines were generated as described above. To determine the proximity localization of RAD54L2 and TOP2A/ZNF451 in cells, PLAs were carried out using a Duolink in situ red starter kit mouse/rabbit (DUO92101-1KT; Sigma-Aldrich) following the manufacturer′s protocol. The primary antibodies used were TOP2A (ab52934; Abcam; 1:400 dilution), ZATT/ZNF451 (NBP2-94743; Novus Biologicals; 1:200 dilution), and FLAG (F3165; Sigma-Aldrich; 1:400 dilution). Images were acquired on a Zeiss LSM880 confocal microscope and analyzed using a custom CellProfiler pipeline. Typically, more than 100 cells were counted per condition from at least two independent biological repeats. For pre-extraction–related PLA, cells were first permeabilized with 0.2% Triton X-100/PBS for 2 min on ice before fixation for PLA experiment.

To determine the chromatin association of RAD54L2 with Immunofluorescence staining, cells were cultured on Falcon 8 well culture slide (354118; Corning). After indicated chemical treatment, cells were first permeabilized with 0.2% Triton X-100/PBS for 2 min on ice, followed by fixation with 4% paraformaldehyde for 20 min at room temperature. Cells were then permeabilized with 0.5% Triton X-100/PBS for 10 min and blocked with 4% BSA/PBS for 1 hour at room temperature. Diluted primary antibodies of FLAG (F3165; Sigma-Aldrich; 1:2000 dilution) and phospho-H2AX (S139, 9718S; Cell Signaling Technology; 1:1000 dilution) in 4% BSA/PBS were then added and incubated at 4°C overnight. At the following day, cells were then incubated with Alexa Fluor Plus 488 goat anti-mouse secondary antibody (A32723; Thermo Fisher Scientific; 1:1000 dilution) and Alexa Fluor Plus 555 goat anti-rabbit secondary antibody (A32732; Thermo Fisher Scientific; 1:1000 dilution) for 1 hour at room temperature. Slides were mounted with Prolong Diamond antifade mountant with 4′,6-diamidino-2-phenylindole (P36971; Thermo Fisher Scientific). Images were acquired on a Zeiss LSM880 confocal microscope and analyzed using a custom CellProfiler pipeline. Typically, more than 100 cells were counted per condition from at least two independent biological repeats.

Recombinant human RAD54L2 production

RAD54L2 cDNA was PCR amplified from a Lenti open reading frame clone of human RAD54L2 purchased from OriGene (RC206881L3) and cloned into Gateway donor vector pDONR201 by BP reaction. RAD54L2 was then subcloned into pLEX_307-SFB by Gateway LR reaction for expression with a C-terminal SFB tag. pLEX_307-RAD54L2-SFB was transfected into HEK293T cells using X-tremeGENE HP DNA Transfection Reagent. Two days after transfection, cells were collected and subjected to purification with streptavidin beads. Basically, collected cells were lysed with ice-cold NETN-100 lysis buffer [50 mM tris-HCl (pH 7.4), 100 mM NaCl, 0.4% NP-40, 1 mM EDTA, and protease inhibitor cocktail] with rotation for 30 min in a cold room. Cell lysates were then clarified by centrifugation at 13,000 rpm for 30 min at 4°C. Supernatants from centrifugation were carefully collected and mixed with pre-equilibrated streptavidin beads for 3 hours in a cold room. After incubation, streptavidin beads were washed with NETN-500 lysis buffer [50 mM tris-HCl (pH 7.4), 500 mM NaCl, 0.4% NP-40, 1 mM EDTA, and protease inhibitor cocktail] twice and then washed with NETN-100 lysis buffer twice, with 10 min for each wash. Biotin diluted in NETN-100 lysis buffer (2 mg/ml) was used to elute RAD54L2-SFB protein from the beads. Eluted proteins were subjected to Coomassie Blue staining for purity check. Protein concentration was determined and stored at −80°C for future use.

For production of recombinant RAD54L2 proteins in insect cells, Bac-to-Bac Baculovirus Expression system (10359016; Thermo Fisher Scientific) was used following the manufacturer′s protocol. In brief, RAD54L2 was cloned into pLEX_307-His-GFP by Gateway LR reaction for expression with a N-terminal His-GFP tag. His-GFP-RAD54L2 was then cloned into pFastBac1. Purified pFastBac1-His-GFP-RAD54L2 plasmids were then transformed into MAX Efficiency DH10Bac competent *E.coli*. Recombinant bacmid DNA were purified and verified by PCR for successful insertion of His-GFP-RAD54L2. His-GFP-RAD54L2 bacmid DNA were transfected into ExpiSf9 cells with ExpiFectamine Sf transfection reagent. P0 viral stock was collected at 120

hours post transfection and was amplified to get P1 viral stock. ExpiSf9 cells were infected with P1 viral for protein expression. Forty-eight hours after the infection of ExpiSf9 cells with P1 viral, cells were collected and washed with ice-cold PBS. Collected cells were lysed with ice-cold NETN-500 lysis buffer [50 mM tris-HCl (pH 7.4), 500 mM NaCl, 0.4% NP-40, 2 mM EDTA, 10 mM $MgCl_2$, 200 U of benzonuclease, and protease inhibitor cocktail] with rotation for 30 min in a cold room. Cell lysates were then clarified by centrifugation at 13,000 rpm for 30 min at 4°C. Supernatants from centrifugation were carefully collected and mixed with pre-equilibrated ChromoTek GFP-Trap agarose (gta; Proteintech) for 3 hours in a cold room. After incubation, ChromoTek GFP-Trap agarose were washed with NETN-500 lysis buffer [50 mM tris-HCl (pH 7.4), 500 mM NaCl, 0.4% NP-40, 1 mM EDTA, and protease inhibitor cocktail] for 10 min, and then benzonuclease buffer [50 mM tris-HCl (pH 8.0), 150 mM NaCl, 2 mM $MgCl_2$, protease inhibitor cocktail, and 50 U of benzonuclease] for 1 hour. After benzonuclease treatment, ChromoTek GFP-Trap agarose was again washed with NETN-500 lysis buffer twice and then Elution buffer [50 mM tris-HCl (pH 7.4), 100 mM NaCl, and 10% glycerol] twice, with 10 min for each wash. RAD54L2 proteins were eluted with Elution buffer containing 60 U of TEV protease for 1 hour at cold room. Protein elute was then incubated with HIS-Select Nickel Affinity Gel (P6611-25ML; Sigma-Aldrich) to eliminate TEV protease from the solution.

Production of recombinant TOP2A proteins in insect cells

For production of recombinant TOP2A proteins in insect cells, similar procedures were carried out as described for RAD54L2, except that TOP2A was expressed with a N-terminal 3FLAG tag with or without a C-terminal 3xSUMO2 tag. 3FLAG-TOP2A, 3FLAG-TOP2A-3xSUMO2, and 3FLAG-TOP2A^{Y805F}-3xSUMO2 were purified with Anti-FLAG Mouse Monoclonal Antibody Agarose Gel (A2220-5ML; Sigma-Aldrich) and eluted with 3x FLAG Peptide.

In vitro FLAG-bead pull-down assay

Insect expressed 3FLAG-TOP2A, 3FLAG-TOP2A-3xSUMO2, or 3FLAG-TOP2A^{Y805F}-3xSUMO2 were prebound to Anti-FLAG Mouse Monoclonal Antibody Agarose Gel as that described in the purification process. The FLAG-beads were then subjected to washes with buffer containing benzonuclease or high salt to eliminate contaminations from DNA or nonspecific proteins. Purified RAD54L2 (1 μg) was then mixed with FLAG-beads only or FLAG-beads bound with 3FLAG-TOP2A, 3FLAG-TOP2A-3xSUMO2, or 3FLAG-TOP2A^{Y805F}-3xSUMO2 in NETN-100 lysis buffer [50 mM tris-HCl (pH 7.4), 100 mM NaCl, 0.4% NP-40, 1 mM EDTA, and protease inhibitor cocktail] for 2 hours. Beads were washed with NETN-100 lysis buffer three times. 2× Laemmli buffer was used to elute all beads bound proteins. Samples were subjected to Western blot or Coomassie Blue staining to detect indicated proteins.

In vitro TOP2cc cleavage assay

TOP2A (25 nM) was incubated with 5 nM pBR322 plasmid, with or without the addition of 100 μM ETO in 20 μl of reaction buffer [50 mM tris-HCl (pH 8), 150 mM NaCl, 10 mM $MgCl_2$, 0.5 mM dithiothreitol, BSA (30 μg/ml), and 2 mM ATP]. RAD54L2 (100 nM) was added as indicated. The reaction was incubated for 20 min at 37°C. Reactions were terminated by addition of SDS. Samples were either boiled with 2× Laemmli buffer for Western blot detection of TOP2Acc and free TOP2A, or digested with proteinase K and loaded onto agarose gel for detection of DNA products.

In vitro TOP2cc decatenation assay

In vitro TOP2cc decatenation assay was conducted using Human Topoisomerase II Assay Kit (TG1001-2; TopoGEN) following the vendor's protocol. In brief, 200 ng of kDNA was incubated with indicated amounts of proteins at 37°C in 20 μl reaction buffer [50 mM tris-HCl (pH 8), 150 mM NaCl, 10 mM $MgCl_2$, 0.5 mM dithiothreitol, BSA (30 μg/ml), and 2 mM ATP]. Reactions were stopped by addition of 4 μl of 5× Stop buffer (5% Sarkosyl, 0.125% bromophenol blue, and 25% glycerol). Samples were loaded directly onto ethidium bromide containing agarose gels.

Data analysis and statistics

All experiments were repeated at least two times, and similar results were obtained. Statistical analysis was performed using GraphPad Prism 8.0.0. A two-tailed unpaired *t* test with Welch's correction was used to perform a statistical analysis of the comparison of two groups.

Supplementary Materials

This PDF file includes:
Figs. S1 to S11
Legends for tables S1 and S2

Other Supplementary Material for this manuscript includes the following:
Tables S1 and S2

REFERENCES AND NOTES

1. J. J. Champoux, DNA topoisomerases: Structure, function, and mechanism. *Annu. Rev. Biochem.* **70**, 369–413 (2001).
2. Y. Pommier, Y. Sun, S. N. Huang, J. L. Nitiss, Roles of eukaryotic topoisomerases in transcription, replication and genomic stability. *Nat. Rev. Mol. Cell Biol.* **17**, 703–721 (2016).
3. L. Uuskula-Reimand, M. D. Wilson, Untangling the roles of TOP2A and TOP2B in transcription and cancer. *Sci. Adv.* **8**, eadd4920 (2022).
4. J. L. Nitiss, Targeting DNA topoisomerase II in cancer chemotherapy. *Nat. Rev. Cancer* **9**, 338–350 (2009).
5. Y. Pommier, E. Leo, H. L. Zhang, C. Marchand, DNA topoisomerases and their poisoning by anticancer and antibacterial drugs. *Chem. Biol.* **17**, 421–433 (2010).
6. A. Canela, Y. Maman, S. Y. N. Huang, G. Wutz, W. Tang, G. Zagnoli-Vieira, E. Callen, N. Wong, A. Day, J. M. Peters, K. W. Caldecott, Y. Pommier, A. Nussenzweig, Topoisomerase II-induced chromosome breakage and translocation is determined by chromosome architecture and transcriptional activity. *Mol. Cell* **75**, 252–266.e8 (2019).
7. N. Sciascia, W. Wu, D. Zong, Y. Sun, N. Wong, S. John, D. Wangsa, T. Ried, S. F. Bunting, Y. Pommier, A. Nussenzweig, Suppressing proteasome mediated processing of topoisomerase II DNA-protein complexes preserves genome integrity. *eLife* **9**, e53447 (2020).
8. J. L. Delgado, C. M. Hsieh, N. L. Chan, H. Hiasa, Topoisomerases as anticancer targets. *Biochem. J.* **475**, 373–398 (2018).
9. Y. Pommier, Drugging topoisomerases: Lessons and challenges. *ACS Chem. Biol.* **8**, 82–95 (2013).
10. A. A. Riccio, M. J. Schellenberg, R. S. Williams, Molecular mechanisms of topoisomerase 2 DNA-protein crosslink resolution. *Cell. Mol. Life Sci.* **77**, 81–91 (2020).
11. Y. Sun, L. M. Miller Jenkins, Y. P. Su, K. C. Nitiss, J. L. Nitiss, Y. Pommier, A conserved SUMO pathway repairs topoisomerase DNA-protein cross-links by engaging ubiquitin-mediated proteasomal degradation. *Sci. Adv.* **6**, eaba6290 (2020).
12. F. C. Ledesma, S. F. El Khamisy, M. C. Zuma, K. Osborn, K. W. Caldecott, A human 5 '-tyrosyl DNA phosphodiesterase that repairs topoisomerase-mediated DNA damage. *Nature* **461**, 674–678 (2009).

13. M. J. Schellenberg, J. A. Lieberman, A. Herrero-Ruiz, L. R. Butler, J. G. Williams, A. M. Muñoz-Cabello, G. A. Mueller, R. E. London, F. Cortés-Ledesma, R. S. Williams, ZATT (ZNF451)-mediated resolution of topoisomerase 2 DNA-protein cross-links. *Science* **357**, 1412–1416 (2017).
14. K. Nakamura, T. Kogame, H. Oshiumi, A. Shinohara, Y. Sumitomo, K. Agama, Y. Pommier, K. M. Tsutsui, K. Tsutsui, E. Hartsuiker, T. Ogi, S. Takeda, Y. Taniguchi, Collaborative action of Brca1 and CtIP in elimination of covalent modifications from double-strand breaks to facilitate subsequent break repair. *PLOS Genet.* **6**, e1000828 (2010).
15. K. C. Lee, K. Padget, H. Curtis, I. G. Cowell, D. Moiani, Z. Sondka, N. J. Morris, G. H. Jackson, S. J. Cockell, J. A. Tainer, C. A. Austin, MRE11 facilitates the removal of human topoisomerase II complexes from genomic DNA. *Biol. Open* **1**, 863–873 (2012).
16. N. N. Hoa, T. Shimizu, Z. W. Zhou, Z. Q. Wang, R. A. Deshpande, T. T. Paull, S. Akter, M. Tsuda, R. Furuta, K. Tsutsui, S. Takeda, H. Sasanuma, Mre11 is essential for the removal of lethal topoisomerase 2 covalent cleavage complexes. *Mol. Cell* **64**, 580–592 (2016).
17. T. Aparicio, R. Baer, M. Gottesman, J. Gautier, MRN, CtIP, and BRCA1 mediate repair of topoisomerase II-DNA adducts. *J. Cell Biol.* **212**, 399–408 (2016).
18. H. Sasanuma, M. Tsuda, S. Morimoto, L. K. Saha, M. M. Rahman, Y. Kiyooka, H. Fujiike, A. D. Cherniack, J. Itou, E. Callen Moreu, M. Toi, S. Nakada, H. Tanaka, K. Tsutsui, S. Yamada, A. Nussenzweig, S. Takeda, BRCA1 ensures genome integrity by eliminating estrogen-induced pathological topoisomerase II-DNA complexes. *Proc. Natl. Acad. Sci. U.S.A.* **115**, E10642–E10651 (2018).
19. Y. Sun, E. Soans, M. Mishina, E. Petricci, Y. Pommier, K. C. Nitiss, J. L. Nitiss, Requirements for MRN endonuclease processing of topoisomerase II-mediated DNA damage in mammalian cells. *Front. Mol. Biosci.* **9**, 1007064 (2022).
20. J. R. Chapman, M. R. G. Taylor, S. J. Boulton, Playing the end game: DNA double-strand break repair pathway choice. *Mol. Cell* **47**, 497–510 (2012).
21. M. C. Haffner, M. J. Aryee, A. Toubaji, D. M. Esopi, R. Albadine, B. Gurel, W. B. Isaacs, G. S. Bova, W. Liu, J. Xu, A. K. Meeker, G. Netto, A. M. de Marzo, W. G. Nelson, S. Yegnasubramanian, Androgen-induced TOP2B-mediated double-strand breaks and prostate cancer gene rearrangements. *Nat. Genet.* **42**, 668–675 (2010).
22. M. Pendleton, R. H. Lindsey Jr., C. A. Felix, D. Grimwade, N. Osheroff, Topoisomerase II and leukemia. *Ann. N. Y. Acad. Sci.* **1310**, 98–110 (2014).
23. F. Gomez-Herreros, DNA double strand breaks and chromosomal translocations induced by DNA topoisomerase II. *Front. Mol. Biosci.* **6**, (2019).
24. N. Rouleau, A. Domans'kyi, M. Reeben, A. M. Moilanen, K. Havas, Z. Kang, T. Owen-Hughes, J. J. Palvimo, O. A. Jänne, Novel ATPase of SNF2-like protein family interacts with androgen receptor and modulates androgen-dependent transcription. *Mol. Biol. Cell* **13**, 2106–2119 (2002).
25. A. Domanskyi, K. T. Virtanen, J. J. Palvimo, O. A. Janne, Biochemical characterization of androgen receptor-interacting protein 4. *Biochem. J.* **393**, 789–795 (2006).
26. B. Linder, R. A. Cabot, T. Schwickert, R. A. W. Rupp, The SNF2 domain protein family in higher vertebrates displays dynamic expression patterns in Xenopus laevis embryos. *Gene* **326**, 59–66 (2004).
27. M. Olivieri, T. Cho, A. Álvarez-Quilón, K. Li, M. J. Schellenberg, M. Zimmermann, N. Hustedt, S. E. Rossi, S. Adam, H. Melo, A. M. Heijink, G. Sastre-Moreno, N. Moatti, R. K. Szilard, A. McEwan, A. K. Ling, A. Serrano-Benitez, T. Ubhi, S. Feng, J. Pawling, I. Delgado-Sainz, M. W. Ferguson, J. W. Dennis, G. W. Brown, F. Cortés-Ledesma, R. S. Williams, A. Martin, D. Xu, D. Durocher, A genetic map of the response to DNA damage in human cells. *Cell* **182**, 481–496.e21 (2020).
28. H. Zhang, Y. Xiong, D. Su, C. Wang, M. Srivastava, M. Tang, X. Feng, M. Huang, Z. Chen, J. Chen, TDP1-independent pathways in the process and repair of TOP1-induced DNA damage. *Nat. Commun.* **13**, 4240 (2022).
29. J. M. Park, H. Zhang, L. Nie, C. Wang, M. Huang, X. Feng, M. Tang, Z. Chen, Y. Xiong, N. Lee, S. Li, L. Yin, T. Hart, J. Chen, Genome-wide CRISPR screens reveal ZATT as a synthetic lethal target of TOP2-poison etoposide that can act in a TDP2-independent pathway. *Int. J. Mol. Sci.* **24**, 6545 (2023).
30. W. Li, H. Xu, T. Xiao, L. Cong, M. I. Love, F. Zhang, R. A. Irizarry, J. S. Liu, M. Brown, X. S. Liu, MAGeCK enables robust identification of essential genes from genome-scale CRISPR/Cas9 knockout screens. *Genome Biol.* **15**, 554 (2014).
31. M. Colic, G. Wang, M. Zimmermann, K. Mascall, M. McLaughlin, L. Bertolet, W. F. Lenoir, J. Moffat, S. Angers, D. Durocher, T. Hart, Identifying chemogenetic interactions from CRISPR screens with drugZ. *Genome Med.* **11**, 52 (2019).
32. S. P. C. Cole, Multidrug resistance protein 1 (MRP1, ABCC1), a "Multitasking" ATP-binding cassette (ABC) transporter. *J. Biol. Chem.* **289**, 30880–30888 (2014).
33. G. Zagnoli-Vieira, K. W. Caldecott, TDP2, TOP2, and SUMO: What is ZATT about? *Cell Res.* **27**, 1405–1406 (2017).
34. T. Tian, M. Bu, X. Chen, L. Ding, Y. Yang, J. Han, X. H. Feng, P. Xu, T. Liu, S. Ying, Y. Lei, Q. Li, J. Huang, The ZATT-TOP2A-PICH axis drives extensive replication fork reversal to promote genome stability. *Mol. Cell* **81**, 198–211.e6 (2021).
35. R. Gao, M. J. Schellenberg, S. Y. N. Huang, M. Abdelmalak, C. Marchand, K. C. Nitiss, J. L. Nitiss, R. S. Williams, Y. Pommier, Proteolytic degradation of topoisomerase II (Top2) enables the processing of Top2.DNA and Top2.RNA covalent complexes by tyrosyl-DNA-phosphodiesterase 2 (TDP2). *J. Biol. Chem.* **289**, 17960–17969 (2014).
36. A. Zhang, Y. L. Lyu, C. P. Lin, N. Zhou, A. M. Azarova, L. M. Wood, L. F. Liu, A protease pathway for the repair of topoisomerase II-DNA covalent complexes. *J. Biol. Chem.* **281**, 35997–36003 (2006).
37. S. Ceruti, A. Mazzola, M. P. Abbracchio, Proteasome inhibitors potentiate etoposide-induced cell death in human astrocytoma cells bearing a mutated p53 isoform. *J. Pharmacol. Exp. Ther.* **319**, 1424–1434 (2006).
38. W. D. Heyer, X. Li, M. Rolfsmeier, X. P. Zhang, Rad54: The swiss army knife of homologous recombination? *Nucleic Acids Res.* **34**, 4115–4125 (2006).
39. O. Barroso-Gomila, F. Trulsson, V. Muratore, I. Canosa, L. Merino-Cacho, A. R. Cortazar, C. Pérez, M. Azkargorta, I. Iloro, A. Carracedo, A. M. Aransay, F. Elortza, U. Mayor, A. C. O. Vertegaal, R. Barrio, J. D. Sutherland, Identification of proximal SUMO-dependent interactors using SUMO-ID. *Nat. Commun.* **12**, 6671 (2021).
40. E. Aguilar-Martinez, X. Chen, A. Webber, A. P. Mould, A. Seifert, R. T. Hay, A. D. Sharrocks, Screen for multi-SUMO-binding proteins reveals a multi-SIM-binding mechanism for recruitment of the transcriptional regulator ZMYM2 to chromatin. *Proc. Natl. Acad. Sci. U.S.A.* **112**, E4854–E4863 (2015).
41. R. Gonzalez-Prieto, K. Eifler-Olivi, L. A. Claessens, E. Willemstein, Z. Xiao, C. M. P. Talavera Ormeno, H. Ovaa, H. D. Ulrich, A. C. O. Vertegaal, Global non-covalent SUMO interaction networks reveal SUMO-dependent stabilization of the non-homologous end joining complex. *Cell Rep.* **34**, 108691 (2021).
42. D. P. Ryan, T. Owen-Hughes, Snf2-family proteins: Chromatin remodellers for any occasion. *Curr. Opin. Chem. Biol.* **15**, 649–656 (2011).
43. F. Aliabadi, B. Sohrabi, E. Mostafavi, H. Pazoki-Toroudi, T. J. Webster, Ubiquitin-proteasome system and the role of its inhibitors in cancer therapy. *Open Biol.* **11**, 200390 (2021).
44. S. L. Harer, M. S. Bhatia, N. M. Bhatia, Proteasome inhibitors mechanism; source for design of newer therapeutic agents. *J. Antibiot.* **65**, 279–288 (2012).
45. Y. Wei, L. X. Diao, S. Lu, H. T. Wang, F. Suo, M. Q. Dong, L. L. du, SUMO-targeted DNA translocase Rrp2 protects the genome from Top2-induced DNA damage. *Mol. Cell* **66**, 581–596.e6 (2017).
46. A. Flaus, T. Owen-Hughes, Mechanisms for ATP-dependent chromatin remodelling: The means to the end. *FEBS J.* **278**, 3579–3595 (2011).
47. K. Kramarz, D. Dziadkowiec, Rrp1, Rrp2 and Uls1-yeast SWI2/SNF2 DNA dependent translocases in genome stability maintenance. *DNA Repair* **116**, 103356 (2022).
48. H. Zhang, Z. Chen, Y. Ye, Z. Ye, D. Cao, Y. Xiong, M. Srivastava, X. Feng, M. Tang, C. Wang, J. A. Tainer, J. Chen, SLX4IP acts with SLX4 and XPF-ERCC1 to promote interstrand crosslink repair. *Nucleic Acids Res.* **47**, 10181–10201 (2019).

Acknowledgments: We thank all members of J.C.'s laboratory for help and constructive discussions and the sequencing and microarray facility at MD Anderson (CA016672) for technical support. **Funding:** This work was supported in part by internal funds that were available to J.C. J.C. also received support from the Pamela and Wayne Garrison Distinguished Chair in Cancer Research, Cancer Prevention & Research Institute of Texas (awards RP160667 and RP180813 to J.C.), and NIH (CA210929, CA216911, and CA216437 to J.C.; P01 CA193124, project 4, to J.C.; and, more recently, CA274234 and CA275712 to J.C.). **Author contributions:** Conceptualization: H.Z., Y.X., Y.S., Y.P., and J.C. Methodology: H.Z., Y.X., and Y.S. Investigation: H. Z., Y.X., Y.S., J.-M.P., D.S., X.F., M.T., M.H., C.W., M.S., C.Y., D.Z., Z.C., S.L., and L.Y. Visualization: H.Z., Y.X., and Y.S. Supervision: Y.P. and J.C. Writing—original draft: H.Z. and Y.X. Writing—review and editing: H.Z., Y.X., S.K., Y.P., and J.C. **Competing interests:** The authors declare that they have no competing interests. **Data and materials availability:** All data needed to evaluate the conclusions in the paper are present in the paper and/or the Supplementary Materials. Requests for reagents should be submitted to J.C. (jchen8@mdanderson.org). Reagents will be provided pending scientific review and a completed material transfer agreement.

Submitted 10 May 2023
Accepted 7 November 2023
Published 6 December 2023
10.1126/sciadv.adi6681